Accuracy Assessment of Numerical Morphological Models based on Reduced Saint-Venant Equations

H.J. Barneveld[1,4], E. Mosselman[2,3], V. Chavarrías[2], A.J.F. Hoitink[1]

[1]Wageningen University and Research, Hydrology and Quantitative Water Management Group, Department of Environmental Sciences, Droevendaalsesteeg 3, 6708 PB Wageningen, the Netherlands
[2]Deltares, P.O. Box 177, 2600 MH Delft, the Netherlands
[3]Delft University of Technology, Faculty of Civil Engineering and Geosciences, P.O. Box 5, 2600 AA Delft, the Netherlands
[4]HKV, Botter 11-29, 8232 JN Lelystad, the Netherlands

Key Points:

- Temporal-mode linear analysis predicts the accuracy of simplified hydrodynamics in 1D numerical morphological models.
- Morphodynamic metrics of quasi-steady models deviate less than 1% from full-dynamic models for Froude numbers up to 0.7.
- Bed wave migration and damping based on the diffusive wave approach are 10% accurate only for Froude numbers of 0.3 or lower.

Corresponding author: Hermjan Barneveld, `hermjan.barneveld@wur.nl`

Abstract

Sustainable river management often requires long-term morphological simulations. As the future is unknown, uncertainty needs to be accounted for, which may require probabilistic simulations covering a large parameter domain. Even for one-dimensional models, the simulation times can be long. One of the strategies to speed up simulations is simplification of models by neglecting terms in the governing hydrodynamic equations. Examples are the quasi-steady model and the diffusive wave model, both widely used by scientists and practitioners. Here, we establish under which conditions these simplified models are accurate. Based on the results of linear stability analyses of the St. Venant-Exner equations, we assess migration celerities and damping of infinitesimal, but long riverbed perturbations. We did this for the full dynamic model, i.e. no terms neglected, as well as for the simplified models. The accuracy of the simplified models was obtained from comparison between the characteristics of the riverbed perturbations for simplified models and the full dynamic model. We executed a spatial-mode and a temporal-mode linear analysis and compared the results with numerical modelling results for the full dynamic and simplified models. The numerical results match best with the temporal-mode linear stability analysis. The analysis shows that the quasi-steady model is highly accurate for Froude numbers up to 0.7, probably even for long river reaches with large flood wave damping. Although the diffusive wave model accurately predicts flood wave migration and damping, key morphological metrics deviate more than 5% (10 %) from the full dynamic model when Froude numbers exceed 0.2 (0.3).

Plain Language Summary

Human interference in rivers impact the transport of sediment in these rivers and cause aggradation and erosion of the riverbed. This may cause problems for navigation, flood safety, groundwater levels, nature, agriculture and stability of infrastructure in and along the river. The changes in the riverbed are called morphological changes, which develop slowly and may continue for hundreds or even thousands of years. For future plans in river basins, it is important to know what the impact of these plans may be on the riverbed development in the future. Numerical models are widely used for this. For simulations of long river reaches and predictive horizons of decades or more, run times of these models can be very large. Shorter run times are possible with simplified models. However, it has remained unclear whether these simplified numerical models provide reliable projections of the future riverbed development. This research provides a method to assess under which conditions of flow and sediment load in the river simplified numerical models can be applied. We prove that a widely used quasi-steady modelling approach yields accurate morphological predictions for a wide range of lowland rivers.

1 Introduction

Human interference in rivers can have large impacts on river morphology that manifests themselves often only after decades, or centuries. Global change and measures to mitigate them or anticipate on these changes (e.g. Haasnoot et al., 2013), have similar time scales. As examples of human induced morphological changes, Havinga (2020), Ylla Arbós et al. (2021), Habersack et al. (2016) and Harmar et al. (2005) describe incising trends in the rivers Rhine, Danube and Mississippi, caused by engineering measures over the past centuries. New (dynamic) equilibrium conditions have not yet been reached. De Vries (1975), Dade and Friend (1998) and Church and Ferguson (2015) show that for lowland rivers, it may take 10^3 to 10^5 years for the riverbed to adapt to permanent changes. This underlines the need for sustainable sediment management in rivers as advocated by Habersack et al. (2016), which requires long-term predictions of the morphological impact of global change and integrated river management strategies for long river reaches. Morphological numerical simulations for river reaches of tens of kilometers over several decades may

take hours to days, even for one-dimensional models. Siviglia and Crosato (2016) provide a list with remaining challenges for numerical modelling of river morphodynamics, including the development of new and fast numerical morphodynamic codes and study of the uncertainty in the results of morphodynamic models. Such new developments will facilitate effective long-term morphological assessments and design of sustainable river management solutions for the next century.

Barneveld et al. (2023) summarized several methods for fast morphological assessments, which include analytical methods, numerical modelling techniques and simplified numerical models in which terms in the governing equations are neglected. They focus on linear stability analyses as a rapid assessment tool for migration and damping of bed waves with spatial scales much larger than the water depth. In combination with numerical simulations and field data, Barneveld et al. (2023) show that especially for moderate and small Froude numbers ($F \leq 0.3$) and bed waves with amplitudes smaller than 10% of the water depth, the linear stability analyses provide a good indication of the morphodynamics of bed waves. The method was verified using field data of the Fraser River in Canada and the Waal River in the Netherlands.

One-, two- and three-dimensional numerical models are potentially capable of simulating long-term morphodynamic developments with a higher degree of resemblance to real-world river geometries than what can be achieved with stability analysis. This is at the cost of a simulation time, which increases with increasing dimension. Concerning techniques for faster numerical modelling techniques, De Vries (1965, 1973) first showed that for lowland rivers with small to moderate Froude numbers ($F < 0.7$), migration celerities of bed perturbations are negligible compared to celerities of hydrodynamic waves. The Saint-Venant equations for water flow and Exner equation for morphological development may then be solved uncoupled. This means that, rather than solving all variables at the same time, one can first resolve the flow (either steady or unsteady) keeping the bed fixed and subsequently solve the bed level keeping the flow fixed. This enables faster simulations. Other researchers (e.g. Lyn, 1987; Morris & Williams, 1996; Lyn & Altinakar, 2002; Cao et al., 2002) confirmed the results of De Vries, yet added the condition of moderate sediment transport as a prerequisite for decoupling.

In addition to the decoupled solution of the set of equations, improvement of numerical solvers, improved CPU performances, parallelization technologies and speeding up of convergence of hydrodynamic computations (e.g. Yossef et al., 2008) are effective in reducing simulation times. Alternatively, one can resort to morphological acceleration factors such as MORFAC (e.g. Lesser et al., 2004; Roelvink, 2006) or MASSPEED (Carraro et al., 2018). These morphological acceleration factors were first introduced for coastal modelling scenarios with cyclical flow, but are also applied for rivers (e.g. Edmonds, 2012; Schuurman & Kleinhans, 2015; Williams et al., 2016). In models using this technique, the bed level changes are multiplied by a non-unity factor after each hydrodynamic time step, thereby extending the morphological time step and thus speeding up simulations.

High computational demands have also motivated efforts to reduce the equations for hydrodynamics, which are typically based on the Saint-Venant equations. The hydrodynamic regime subject to study determines which type of simplifications may be allowed. Grijsen and Vreugdenhil (1976) distinguish short inertial or gravity waves, in which friction is neglected, diffusive waves, where inertia is neglected, and kinematic waves, where inertia and non-uniformity are neglected. Ponce and Simons (1977) added the steady dynamic wave, in which only the time derivative in the momentum equation of flow is neglected. The appropriateness of omitting terms in the equations of motion depends on the type of problem. For flood forecasting, kinematic wave models (e.g. Singh, 2001; Lee & Huang, 2012; Chen & Capart, 2020) and diffusive wave models (e.g. Cappelaere, 1997; Moussa & Bocquillon, 2009) are widely used. Teng et al. (2017) show that such simplified modelling approaches are also applicable to 2D flood inundation modelling. Both

Grijsen and Vreugdenhil (1976) and Ponce and Simons (1977) apply linear stability analyses to assess the error of hydrodynamics of simplified models compared to models based on the full set of equations (unsteady or full-dynamic models). They prove, for example, that the diffusive wave model can accurately simulate the celerity and damping of flood waves in rivers.

Simplified hydrodynamic models can be used in combination with the Exner equation to form simplified morphological models. Examples of numerical morphological models based on the diffusive wave approach are described in Fasolato et al. (2011) and Abril et al. (2012). One simplification has become particularly popular both in scientific literature and in consultancy practice, which is referred to as the quasi-steady approach. Under this assumption, the flow can be considered steady during subsequent morphodynamic steps of the decoupled solution procedure. This implies that the time derivatives in both Saint-Venant equations are neglected. The discharge may still vary in time, but during one time step, the discharge is the same for the entire river.

Although flood wave attenuation in long river models is not captured in a quasi-steady model, the quasi-steady approach has obtained a wide application domain. Cao et al. (2017) mention that quasi-steady flow models are frequently used by Chinese engineers for large-scale and long-duration cases such as the operation of the Three Gorges Reservoir in the Yangtze River. The quasi-steady approach is also implemented in commercial one-dimensional software packages such as HEC-RAS, MIKE 11 and SOBEK-RE. The advantage of the quasi-steady approach over the unsteady approach is related to the larger time step that can be used in the quasi-steady models. In the HEC-RAS manual (USACE, 2022) the quasi-steady model is described as more stable than the unsteady model. Although the unsteady flow engine is faster than the quasi-steady flow engine, a variable time step feature in HEC-RAS and stricter time step requirements for the stability of unsteady hydraulics lead to shorter quasi-steady model runs. Thanks to the backwater curve simulations for the flow in the quasi-steady mode, the Courant-Friedrichs-Lewy (CFL) condition may be based on the celerity of disturbances in the riverbed in both MIKE 11 and SOBEK-RE. As these celerities are much lower than celerities of water level disturbances, this allows for a much larger time step. The MIKE 11 manual (DHI, 2017) states that the time step in the quasi-steady mode often will be limited only by the ability to resolve the boundary conditions.

In SOBEK-RE of Deltares (the Netherlands) the hydrodynamics are calculated using an implicit Preissmann scheme and the morphology scheme is explicit. Running the model in unsteady mode means that the time step is restricted by reproducing the boundary conditions and by accuracy. As a rule of thumb, simulations with a time step restricting the hydraulic Courant number to a maximum value of 10 provide accurate and stable results (pers. comm. C.J. Sloff, 2022). In the quasi-steady mode of SOBEK-RE, the celerity of riverbed disturbances determines the (morphological) Courant number. As the morphological celerities are generally low, the time step is restricted only by proper representation of the hydraulic wave in most cases. This time step is normally much larger than the time step for unsteady simulations, which is restricted by the criterion CFL $<$ 10. As the solvers for the unsteady and quasi-steady models are comparably efficient, the quasi-steady simulations with SOBEK-RE can be up to dozens of times faster than the unsteady simulations.

Regarding the maximum time step for morphological simulations, Vreugdenhil (1994) proves that for large hydraulic Courant numbers implicit schemes are becoming less accurate. Vreugdenhil (1982) and Olesen (1981) show that the maximum Courant number (and thus time step Δt) depends on the numerical method, spatial discretization (Δx) and targeted morphological accuracy. They show that to maintain a certain degree of accuracy in implicit schemes, larger Courant numbers are possible, but with increasing Courant number, a higher spatial discretization (smaller Δx) is required. Consequently also the time step is restricted. Van Buuren et al. (2001) performed numerical simula-

tions with a second-order implicit Crank–Nicolson scheme, and showed that for acceptable accuracy, the time step may be not more than 20 to 40 or even 80 times larger than the explicit stability time step following from the hydrodynamic CFL condition.

The analysis of prevailing quasi-steady morphological numerical codes shows that although the solvers for the quasi-steady models are not faster than those of the unsteady models, simulations with quasi-steady models can be substantially faster due to the possibility of larger time steps and a schematized hydrograph. However, quasi-steady models do not simulate damping of flood waves, which may result in underestimation of morphological changes in long river models. In such cases, diffusive wave models better simulate the flood wave dynamics and possibly also the morphological changes. Although for specific field cases unsteady and simplified models are sometimes compared (e.g. Hummel et al., 2012; Sloff, 2000), it remains unknown under which circumstances common simplified morphological models exactly apply. Here, we aim to establish under which conditions the quasi-steady model and diffusive wave model yield accurate morphological predictions, even when these rivers are very long. We perform linear stability analyses on the 1-dimensional set of equations and verify these with numerical simulations to assess the ranges of Froude numbers, sediment loads and bed wave dimensions for which simplified models (i.e. quasi-steady model and diffusive wave model) can be applied. In addition we perform numerical simulations to assess the importance of flood wave damping in longer river stretches on the morphological predictions of quasi-steady models.

The structure of the remainder of this paper is as follows. Section 2 describes the linear stability analyses, providing analytical expressions of migration celerity and damping for the unsteady and simplified models. The same section describes the simulations performed with the numerical model ELV. Results of the linear stability analysis, the comparison with numerical results and assessment of the validity range of simplified numerical models are given in Section 3 and further discussed in Section 4. Section 5 summarizes the main conclusions.

2 Methods

2.1 Model Equations

We consider unidirectional flow over an erodible bed and we interpret bed elevation and sediment transport per unit width to be averaged over smaller bedforms (ripples and dunes) for which the impact on flow conditions is incorporated through a roughness parameter. We consider the development of large perturbations or bed waves in the riverbed, with wave lengths much larger than the water depth. For these conditions the one-dimensional governing equations describing flow and bed evolution read as:

$$\alpha_1 \frac{\partial u}{\partial t} + \alpha_2 u \frac{\partial u}{\partial x} + g\frac{\partial h}{\partial x} + g\frac{\partial z}{\partial x} = -g\frac{u^2}{C^2 h} \tag{1}$$

$$\beta \frac{\partial h}{\delta t} + h\frac{\partial u}{\partial x} + u\frac{\partial h}{\partial x} = 0 \tag{2}$$

$$\frac{\partial z}{\partial t} + \frac{\partial s}{\partial x} = 0 \tag{3}$$

$$s = f(u) \tag{4}$$

Herein:
t = time (s)
x = longitudinal co-ordinate (m)

u = water velocity averaged in a cross-section (m/s)
h = water depth (m)
z = bed level (m)
C = Chézy coefficient for hydraulic roughness ($m^{1/2}/s$)
s = sediment transport per unit of width (bulk volume) (m^2/s)
g = acceleration due to gravity (m/s^2)
α_i (i = 1, 2) and β are flag integers that can take values of 0 and 1 only.

This set of equations contains the 1D Saint-Venant equations for conservation of mass and momentum of water (Eq. 1 and Eq. 2), the continuity equation for sediment (Eq. 3) and a capacity-limited sediment transport predictor (Eq. 4), implicitly assuming small bed slopes. The latter two equations together form the Exner equation. For the case of long bed waves, equilibrium sediment transport predictors such as Meyer-Peter and Müller (1948) or Engelund and Hansen (1967) are widely used. Here, we adopt the latter formula, which is especially suitable for lowland sand-bed rivers. It relates the equilibrium sediment transport capacity to the flow velocity ($s = m\ u^n$). The parameter m depends on the sediment properties (median grain diameter and density) and hydraulic roughness. The power n equals 5.

For the full dynamic model all values of α_i and β are equal to 1. When in the Saint-Venant equations the time derivatives are neglected (α_1=β=0), Eq. 2 reduces to $\frac{\partial q}{\partial x} = 0$, representing steady flow conditions for every time step. In numerical models the discharge may still vary over time, hence the name quasi-steady model (e.g. De Vries, 1973; Sieben, 1996; Yossef et al., 2008; Paarlberg et al., 2015; Guerrero et al., 2015). Another often applied simplified model neglects both inertial terms in Eq. 1 (α_1=α_2=0). In flood routing and morphodynamics this is often called the diffusive wave model. This model has been known accurate for a long time in predicting migration and damping of flood waves in lowland rivers (e.g. Grijsen & Vreugdenhil, 1976; Ponce & Simons, 1977) and has been extensively analyzed (e.g. Cappelaere, 1997; Moussa & Bocquillon, 2009; Charlier et al., 2019; Beg et al., 2022) and applied for hydrological studies since then (e.g. Fan & Li, 2006; Cimorelli et al., 2018; Fenton, 2019; Mitsopoulos et al., 2022).

2.2 Linear Stability Analysis

Barneveld et al. (2023) present linear stability analyses that are valid for bed waves with wave lengths much larger than the water depth. The analyses are based on equations 1 through 4 with all values of α_i and β equal to 1 (full dynamic model), and small perturbations of water depth, flow velocity and bed level:

$h = h_o + h'$
$u = u_o + u'$
$z = z_o + z'$

The subscript o indicates the steady uniform reference situation and the superscript $'$ indicates a small perturbation to the steady uniform reference situation. Substituting these expressions for h, u and z in equations 1 through 4 and assuming a periodic solution such as

$$\begin{bmatrix} u' \\ h' \\ z' \end{bmatrix} = \begin{bmatrix} \hat{u} \\ \hat{h} \\ \hat{z} \end{bmatrix} e^{ikx - i\omega t} \tag{5}$$

yields a set of equations for which solutions are given by

$$\begin{vmatrix} A_r + iA_i & D_r + iD_i & F_r + iF_i \\ B_r + iB_i & E_r + iE_i & 0 \\ C_r + iC_i & 0 & G_r + iG_i \end{vmatrix} = 0 \tag{6}$$

where

$$A_r = \alpha_1\omega_i - \alpha_2 u_o k_i + 2\frac{g i_o}{u_o} \qquad A_i = -\alpha_1\omega_r + \alpha_2 u_o k_r$$
$$B_r = -h_o k_i \qquad B_i = h_o k_r$$
$$C_r = b - \frac{q_{so}}{u_o}k_i \qquad C_i = b\frac{q_{so}}{u_o}k_r$$
$$D_r = -gk_i - \frac{g i_o}{h_o} \qquad D_i = gk_r$$
$$E_r = \beta\omega_i - u_o k_i \qquad E_i = -\beta\omega_r + u_o k_r$$
$$F_r = -gk_i \qquad F_i = gk_r$$
$$G_r = \omega_i \qquad G_i = -\omega_r$$

and

$\hat{u}$, $\hat{h}$, $\hat{z}$ = velocity, depth, bed level amplitude function (-)
k = complex wave number (m^{-1})
ω= complex frequency (s^{-1})
$i = \sqrt{-1}$

To solve Eq. 6, two approaches are possible, a spatial-mode linear stability analysis or a temporal-mode linear stability analysis. In the spatial-mode analysis, the wave number k in the periodic solution is assumed complex and the wave frequency ω in the periodic solution is real and equal to $\omega_r = \frac{2\pi}{T}$, where T is the wave period. In the temporal-mode analysis, the frequency ω is assumed complex and the wave number is real and equal to $k_r = \frac{2\pi}{L}$, where L is the wave length. The complex roots, i.e. either ω or k, determine the propagation and damping of perturbations in the flow and at the riverbed.

A spatial-mode analysis fits best to a model in which oscillating boundary conditions exert an influence on the modelling domain of interest. Temporal-mode analyses are appropriate for systems with initial conditions in infinitely long domains (i.e. Drazin & Reid, 2004) or at least for reaches far away from boundaries. Both situations are relevant for river systems, so we explore both methods.

In Barneveld et al. (2023), a similar method has been described in which the linearized expressions for h, u and z were inserted in equations 1 through 4 before combining these four equations into a single equation in one of the parameters. The resulting third order equation (for the full dynamic model) can again be solved analytically by assuming a periodic solution (like Eq. 5).

For the spatial-mode analysis of the full dynamic model, Barneveld et al. (2023) derived a third-order algebraic equation in the dimensionless wave number $\hat{k}$ (Eq. 12 in Barneveld et al. (2023), for the case α_1=α_2=β=1):

$$\frac{\Psi}{2\pi F^3 E}(\hat{k})^3 + \frac{1}{F^3 E}(1 - \alpha_2 F^2 + \beta\Psi)(\hat{k})^2 - \frac{\alpha_1 + \alpha_2\beta}{2}\frac{4\pi}{FE}\hat{k} + 3i\hat{k} - \alpha_1\beta\frac{4\pi^2}{FE} + 4\pi i = 0 \tag{7}$$

where:

$$\hat{k} = \hat{k}_r + i\hat{k}_i = kx_o\ (-) \tag{8}$$

$$x_o = \frac{Q_o T}{B_o h_o} = u_o T \text{ (m)} = \quad \text{characteristic length scale} \tag{9}$$

Herein, Q_o is the undisturbed water discharge, and B_o is the undisturbed width. This method identifies the three governing dimensionless parameters F, Ψ and E:

$$F = \frac{u_o}{\sqrt{g h_o}} = \quad \text{Froude number} \tag{10}$$

$$\Psi = n\frac{s_o}{q_o} = \quad \text{dimensionless transport parameter} \tag{11}$$

$$E = \sqrt{\frac{g^3 T^2}{C^4 h}} = \quad \text{dimensionless flow variation parameter} \tag{12}$$

The parameter E expresses the influence of unsteadiness and non-uniformity of the flow on a scale larger than the local flow depth.

The three roots of Eq. 7 determine the characteristic wave properties (migration celerity c and damping length L_d) of water and bed waves:

$$c = -\frac{2\pi u_o}{\hat{k}_r} \tag{13}$$

$$L_d = \frac{u_o T}{\hat{k}_i} = \frac{u_o E C^2 h^{1/2}}{\hat{k}_i g^{3/2}} \tag{14}$$

where L_d is defined as the distance over which the amplitude of a wave is damped by a factor e^{-1}. As in subcritical conditions the migration celerity of bed waves is much lower than the one of water waves, the morphodynamic root can easily be identified.

For the temporal-mode analysis of the full dynamic model, Barneveld et al. (2023) presented a third-order algebraic equation in the dimensionless complex frequency $\hat{\omega}$ (Eq. 21 in Barneveld et al. (2023), when α_1=α_2=β=1):

$$\alpha_1\beta F^2(\hat{\omega})^3 + (2i - 2\frac{\alpha_1+\alpha_2\beta}{2}\hat{L}F^2)(\hat{\omega})^2 + (-3\hat{L}i - (\hat{L})^2(1-\alpha_2F^2+\beta\Psi))\hat{\omega} + (\hat{L})^3\Psi = 0 \tag{15}$$

where:
$\hat{L} = 2\pi\frac{L_o}{L}$ (-)
$L_o = \frac{h_o}{i_o}$ (m)
L = wave length of disturbance (m)
Herein, $\hat{\omega} = \hat{\omega}_r + i\hat{\omega}_i$ = dimensionless complex frequency (-)

Clearly in the temporal-mode analysis the governing parameters are Froude number F, transport parameter Ψ and bed wave length L. Solving Eq. 15 again provides the roots determining propagation and damping of disturbances of flow and the bed.

$\hat{\omega}_r$ determines the migration celerity of the waves (water and bed waves), according to:

$$c = \frac{L}{T} = \frac{\hat{\omega}_r u_o}{\hat{k}}. \tag{16}$$

and $\hat{\omega}_i$ determines the damping of water and bed waves:

$$L_d = -\frac{c}{\hat{\omega}_i} \tag{17}$$

For the quasi-steady model Eq. 7 and Eq. 15 provide, with α_1=β=0 and α_2=1, a second order equation. For the diffusive wave model, with α_1=α_2=0 and β=1, a (simplified) third order equation results.

Solving these equations, or directly solving the matrix in Eq. 6, yields roots for the complex wave number (spatial-mode analysis) or complex frequency (temporal-mode analysis) for the different models. With equations 13 and 14 for the spatial-mode analysis and equations 16 and 17 for the temporal-mode analysis, the migration celerity and damping length of bed waves can be determined. The ratio of parameters for the simplified models and those of the full dynamic model determine how accurate the simplified models are, using that the full dynamic model provides the proper values for migration celerity and damping. These ratios are defined as follows for the spatial-mode analysis:

$$c_\mathrm{b} = \frac{c_\mathrm{simplified}}{c_\mathrm{full\ dynamic}} = \frac{\hat{k}_\mathrm{r,full\ dynamic}}{\hat{k}_\mathrm{r,simplified}} \tag{18}$$

$$L_\mathrm{b} = \frac{L_\mathrm{simplified}}{L_\mathrm{full\ dynamic}} = \frac{\hat{k}_\mathrm{i,full\ dynamic}}{\hat{k}_\mathrm{i,simplified}} \tag{19}$$

For the temporal-mode analysis the ratios are

$$c_\mathrm{b} = \frac{\hat{\omega}_\mathrm{r,simplified}}{\hat{\omega}_\mathrm{r,full\ dynamic}} \tag{20}$$

$$L_\mathrm{b} = \frac{\hat{\omega}_\mathrm{i,full\ dynamic}}{\hat{\omega}_\mathrm{i,simplified}} \tag{21}$$

2.3 Numerical Model Simulations

2.3.1 Introduction

To verify whether the results of the linear stability analysis can be used to assess the applicability of simplification of hydrodynamics in morphological models, numerical model simulations are performed for both infinitesimal perturbations and large-amplitude perturbations in the riverbed. The cases performed in Barneveld et al. (2023) form the starting point for the simulations. For this study, these cases were also performed with the quasi-steady model and the diffusive wave model.

2.3.2 Model Description

Barneveld et al. (2023) selected the numerical modelling code ELV (Chavarrías, Stecca, et al., 2019), which is a Matlab code for modelling morphodynamic processes on a one-dimensional domain. ELV has been applied successfully in various studies and proved stable and accurate (Arkesteijn et al., 2019, 2021; Blom et al., 2017; Chavarrías, Arkesteijn, & Blom, 2019). The full set of equations (1 through 4) are solved in an uncoupled way, with an implicit Preissmann scheme for flow and a first-order forward Euler upwind scheme for morphology. In Barneveld et al. (2023) the results of the full dynamic model have already been presented and for validation compared with the extensively tested and widely applied SOBEK-RE model. ELV also provides code for the simplified quasi-steady and diffusive wave models.

2.3.3 Model Set-Up

The model set-up is identical to and extensively described in Barneveld et al. (2023), with a one-branch model for which the geometry is inspired on the Meuse River in the Netherlands (Table 1).

Table 1. Model set-up for simulation with ELV, ranges of parameters depending on cases simulated (Barneveld et al., 2023)

Characteristic	Value/description
model length	10-25 km
channel width (no floodplains) B	100 m
hydraulic roughness, Chézy value C	40 $m^{1/2}/s$
bed slope i_b	0.0001 to 0.0022 (giving Froude numbers up to 0.6)
space step Δx	2.5-25 m
time step Δt	1-5 s
sediment transport s	uniform sediment, transport predictor of Engelund and Hansen (1967)
grain diameter $D50$	0.002 to 0.35 m (to maintain constant Ψ)
upstream boundary conditions	time series for discharge with base flow of 500 m^3/s and equilibrium sediment transport
downstream boundary condition	uniform flow conditions (stage-discharge relation for uniform flow)

2.3.4 Performed Simulations

The simulations performed are taken from Barneveld et al. (2023), which are valid for conditions in lowland rivers. The Froude number F varies between 0.1 and 0.6. For the dimensionless transport parameter Ψ a constant value of 5.15 $\cdot 10^{-5}$ was set, which means that for increasing Froude number the grain size increases. The parameter E is determined by the wave period of the flood wave, which we set at 25 days in a 45 days time domain.

The first set of simulations is based on combinations of the parameters F, E, Ψ for which a value of the wave length of (low) bed perturbations was selected, matching the spatial-mode linear stability analysis. The wave lengths of these low bed perturbation vary from 107 m (F=0.1) to 446 m (F=0.6). In further sets of the simulations the wave length (set 2) and the amplitude of the bed perturbations were increased (set 3). The set of simulations performed is shown in Table 2.

Table 2. Numerical simulations performed to validate results from the linear stability analysis (Barneveld et al., 2023).

Set	Qbase[a] (m^3/s)	Qtop[b] (m^3/s)	Height[c] (m)	Length[d] (m)	Run duration (yr)	Comment
1	500	505	0.005	matching to flow (107-446 m)	1	base set
2	500	505	0.005	3000	3	long bed wave
3	500	1500	0.1-0.5	3000	3	large flow and bed waves

[a]base flow boundary condition
[b]peak flow boundary condition
[c]height of bed perturbation (bed wave)
[d]wave length of bed perturbation (bed wave)

The impact of flood wave damping on the morphological effects is not captured by the quasi-steady model. In case of strong damping of the flood wave, the quasi-steady model will overestimate the peak discharge and underestimate the duration of the flood wave in downstream reaches. This may alter the morphological response. With the quasi-steady model we performed test simulations with an original and attenuated flood wave, having the same water volume, to assess this impact.

3 Results

3.1 Migration Celerity of Bed Perturbations

For the spatial-mode analysis, the ratio of migration celerity for simplified and full dynamic models can be assessed with Eq. 18 for combinations of the parameters E, F and Ψ. For the temporal-mode analysis, Eq. 20 provides this ratio for combinations of the parameters F, Ψ and L. These ratios can be assessed as well with the numerical simulation results for the same combinations of parameters. From the numerical results the migration celerities are taken from the propagation of the top of the perturbation. Figure 1 shows an example of the migration of perturbations for the alternative numerical models and Figure 2 shows the matching average migration celerities according to the three models.

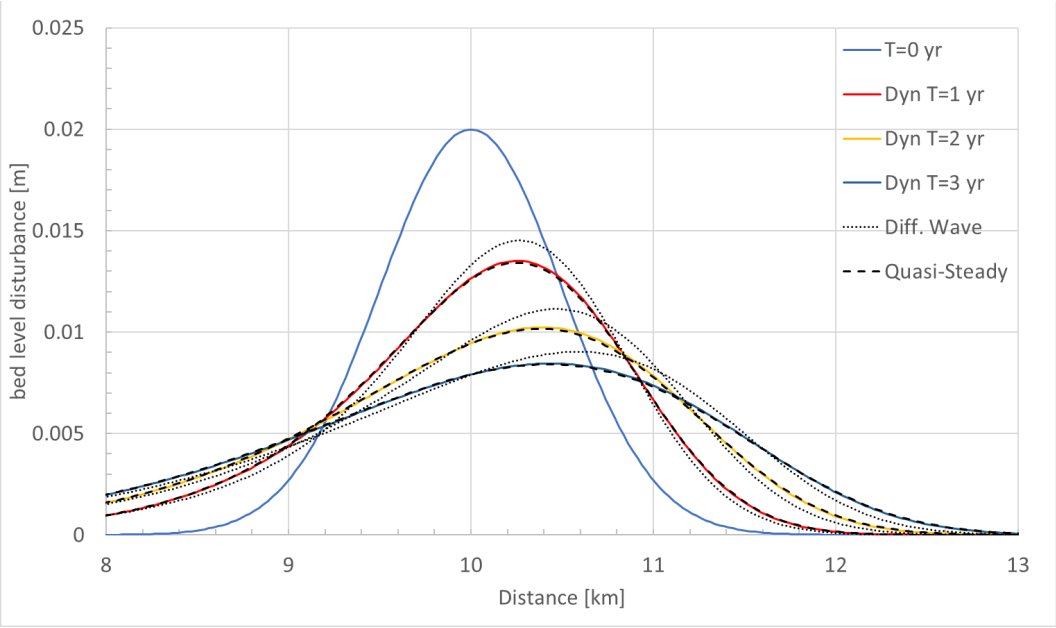

Figure 1. Simulation results for three models Dyn=Full Dynamic Wave model; Diff.Wave= diffusive wave model and the quasi-steady model for the case of F=0.5, $\Psi = 5.15 \cdot 10^{-5}$ and sediment perturbation of 2 cm high and 3 km long.

The results from the linear stability analyses and the numerical results for the infinitesimal perturbations (set 1 in Table 2) are shown in Figure 3. For the quasi-steady model, the results from the linear stability analyses match perfectly well. Clearly, the numerical results for the initial celerities (t=0 yr) are in good agreement with the spatial-mode analysis in the area delimited by the lines for E=10,000 (F=0.1) and E=30,000 (F=0.6). Also, the numerical results are in line with the temporal-mode analysis.

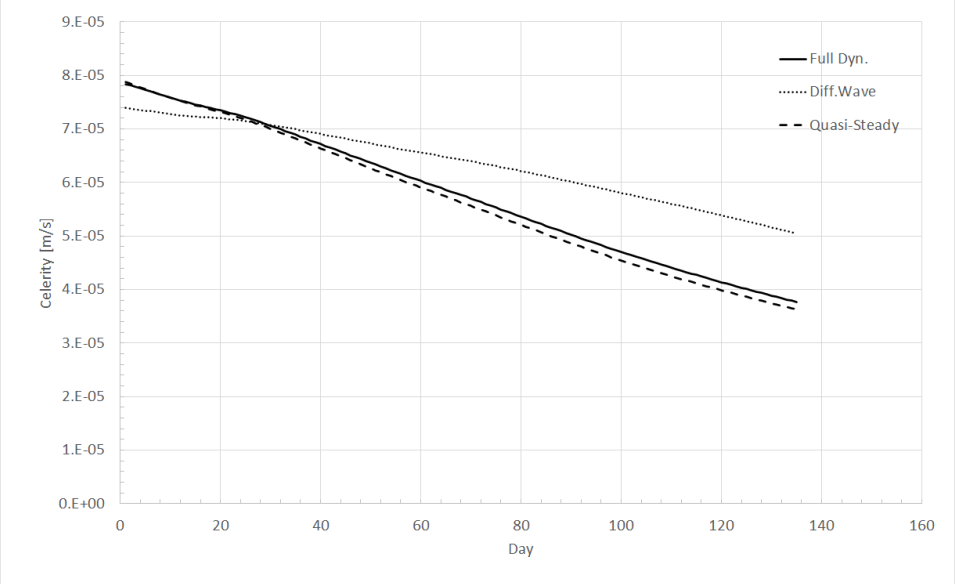

Figure 2. Migration celerity of the riverbed perturbation for the three models shown in Figure 1. The lines show the average celerities of the peak of the perturbation after x days.

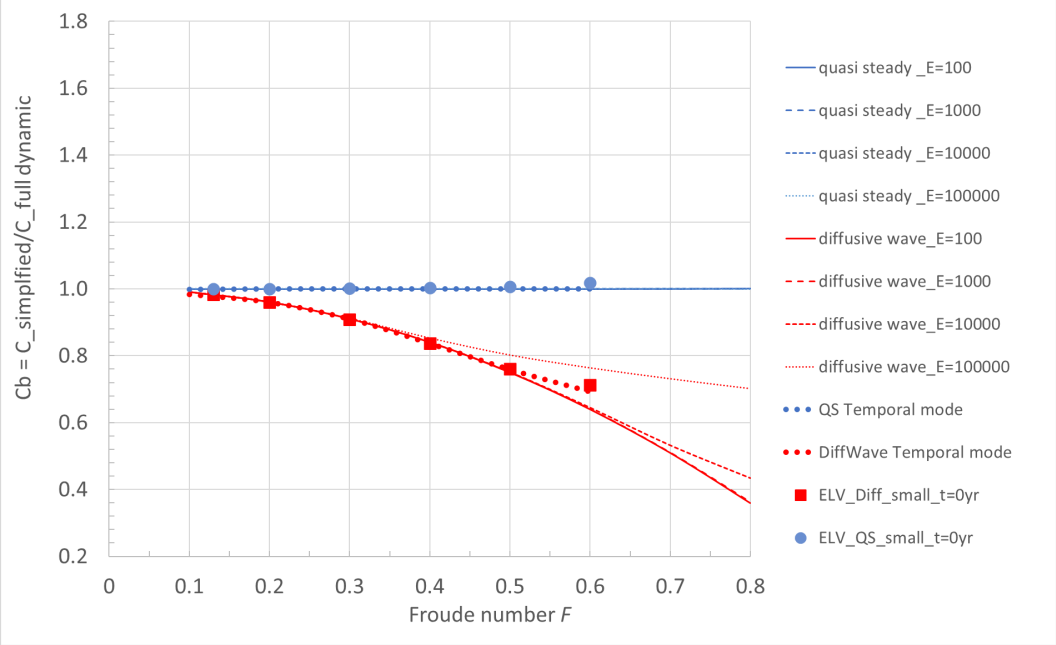

Figure 3. Ratio of celerity of simplified models to full dynamic model for linear stability analyses and numerical results of simulations of small riverbed perturbations, $\Psi = 5.15 \cdot 10^{-5}$.

When longer bed perturbations with a wave length of 3,000 m are considered, with the amplitude still chosen small (set 2 in Table 2), Figure 3 changes to Figure 4. The numerical results for the diffusive wave model fit better to the temporal-mode linear stability analysis. For the diffusive wave model, the ratio according to the spatial-mode analysis is always smaller than unity, while the temporal-mode analysis follows the numerical results in the change of the ratio from below 1 to over 1, when F increases.

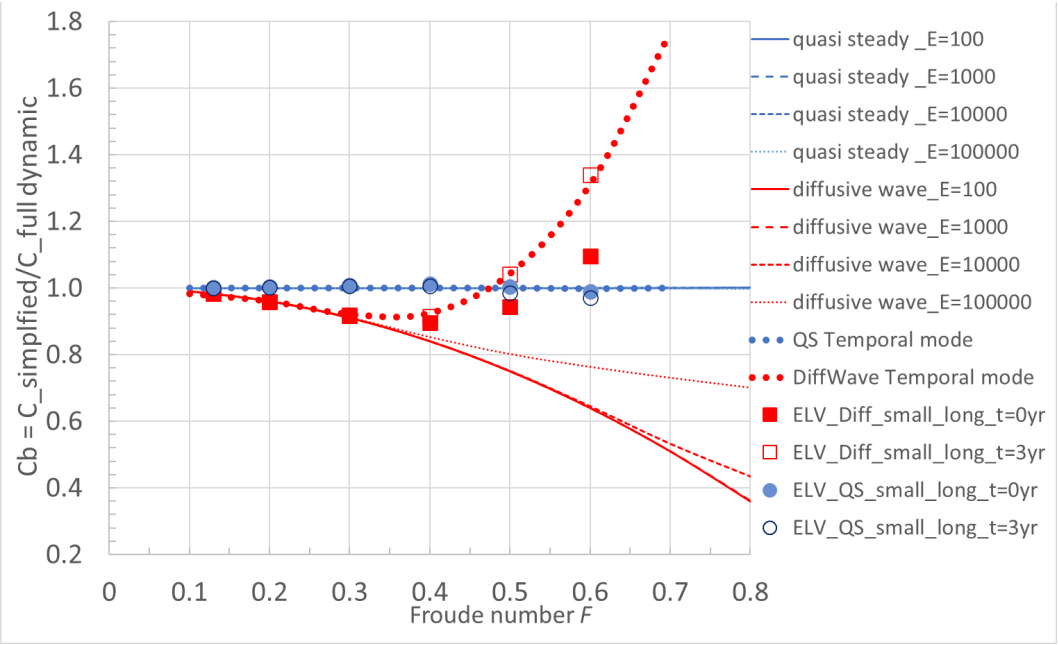

Figure 4. Ratio of celerity of simplified models to full dynamic model for linear stability analyses and numerical results for 3,000 m long but still low amplitude ($\leq$ 0.025 m) bed perturbations, $\Psi = 5.15 \cdot 10^{-5}$.

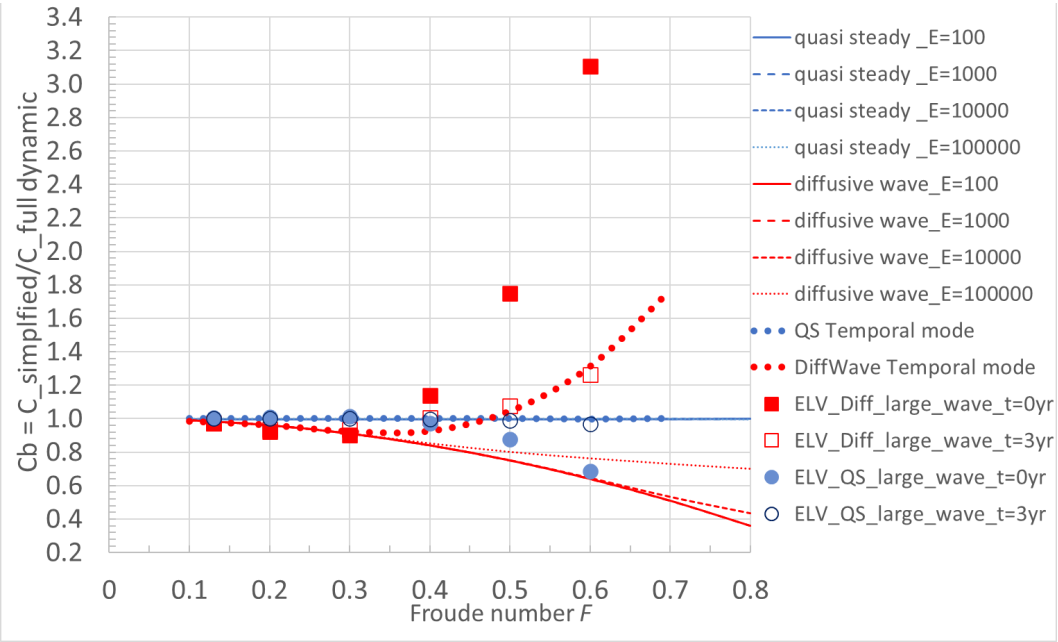

Figure 5. Ratio of celerity of simplified models to full dynamic model for linear stability analyses and numerical results for long and large bed perturbations under a flood wave regime, $\Psi = 5.15 \cdot 10^{-5}$.

When the amplitude of the perturbations also increases (to a maximum of 0.5 m) and a flood wave with a period of 25 days and peak discharge of 1,500 m^3/s is resolved,

the figure further evolves to Figure 5 (note the change in vertical scale compared to Figure 4). Although the ratio of initial migration celerities from the numerical models deviate more from the temporal-mode analysis, the results after three years of simulation are quite similar. Apparently, the temporal-mode analysis is again closer to the numerical results for the diffusive wave model. However, for the quasi-steady model, both approaches in linear stability analysis yield accurate metrics for the accuracy estimate of that simplified model (blue lines and markers).

3.2 Damping of bed perturbations

Figure 1 shows how in subcritical conditions a bed wave dampens when migrating downstream. Such damping in the numerical model is also described by the spatial-mode analysis (Eq. 14) and temporal-mode analysis (Eq. 17). Combining the results of the linear stability analyses (Eq. 19 respectively Eq. 21) and the numerical results from the cases in Figure 3 and Figure 5 provides Figure 6. This figure shows the ratio of damping length of the simplified models to the damping length of the full dynamic model. Again, the results of the linear stability analyses for the quasi-steady model overlap.

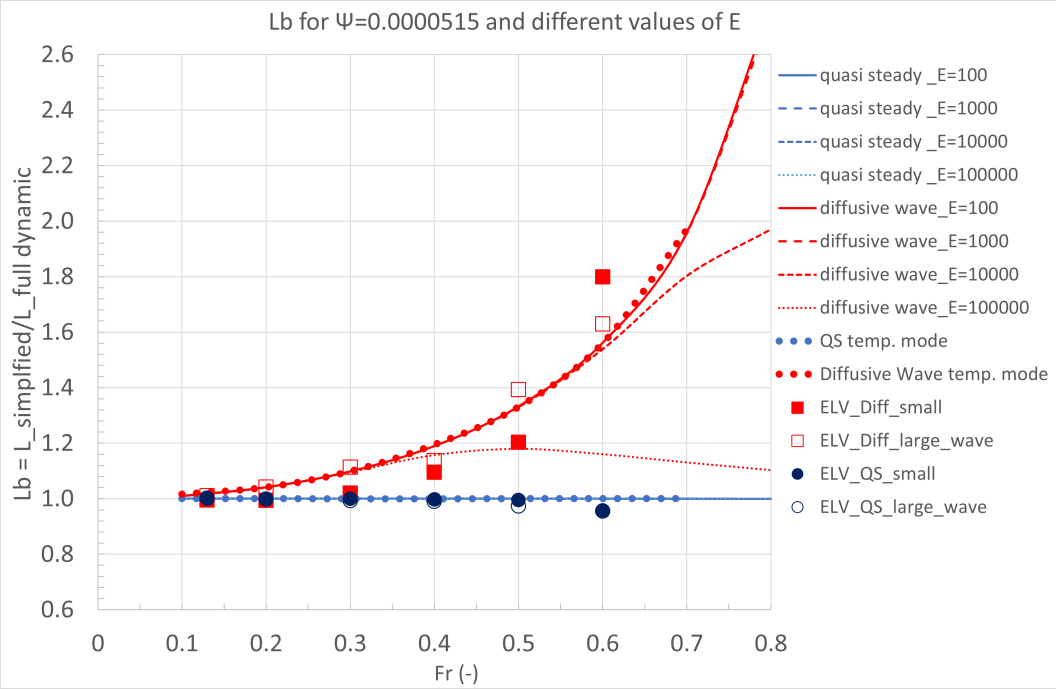

Figure 6. Ratio of damping length of simplified models to full dynamic model for linear stability analyses and numerical results for small bed perturbations (filled markers) as well as for long and large bed perturbations under a flood wave regime (open markers). Thin lines represent the spatial-mode analysis and the thick dotted lines provide temporal-mode analysis results, $\Psi = 5.15 \cdot 10^{-5}$.

Figure 6 shows that spatial-mode and temporal-mode analyses closely align when the Froude number F is less than or equal to 0.4. The numerical results show that the distance over which the amplitude of a wave is damped by a factor e^{-1} is not clearly dependent on the height of the bed perturbation. Finally, the linear stability analyses results are close to the numerical simulation results, especially in case of the temporal-mode analysis. For the diffusive wave model, the spatial-mode analysis with values of E be-

ing well over 100,000 (as indicated by Barneveld et al. (2023)), underestimates the damping length ratio compared to the numerical results, especially for Froude numbers larger than 0.4.

3.3 Impact of flood wave damping on quasi-steady model results

Figure 7 shows boundary conditions for the simulations with original and attenuated flood waves and the corresponding morphological changes simulated with the quasi-steady model. The case represents a typical flood wave attenuation in the Meuse River in the Netherlands. Figure 7 (b) shows that the lines for the two simulations overlap, so the resulting morphodynamics appear to be identical for this case.

4 Discussion

4.1 Spatial-Mode or Temporal-Mode Analysis

In Barneveld et al. (2023) it was shown that the spatial-mode linear stability analysis of one-dimensional riverbed evolution provides accurate information on the initial migration celerities of small bed perturbations (several hundreds of meters long and low amplitude) in case of the full dynamic model. They also showed that for longer and higher bed perturbations the spatial-mode analysis still describes the initial migration celerities well, but overestimates the long-term migration celerities when F is larger than 0.3. In this context the temporal-mode analysis performs better. These ranges are also reflected in the ratios of migration celerities of bed waves as presented in Figures 3, 4 and 5. For both types of reduced equations models, the ratios of initial migration celerities are well-described by the spatial-mode analysis for $F \leq 0.3$. For larger Froude numbers, the spatial-mode analysis underestimates the ratio for migration celerities in case of the diffusive wave model, even at the initial stage. This underestimation grows with increasing Froude number.

The convective (or advective) acceleration term ($u\ \frac{\partial u}{\partial x}$) in the hydrodynamic momentum equation (Eq. 1), which is neglected in the diffusive wave model (α_2=0), appears to be important for proper calculation of the migration celerity of bed waves. Grijsen and Vreugdenhil (1976) and Ponce and Simons (1978) showed that for flood wave conditions in rivers, the convective acceleration term does not have important impact on the celerity and damping of flood waves over a flat riverbed. In combination with a bed wave, the term does become important for the morphodynamics of that bed wave. In the spatial-mode analysis, neglecting the convective acceleration term causes an overestimation of the diffusion coefficient $D = \frac{h_o u_o}{2 i_o}(1 - \alpha_2 F^2 + \frac{\beta}{h_o}\ \frac{\partial f(u)}{\partial u}\Big|_o)$ in Eq. 5 of Barneveld et al. (2023) as α_2=0. This overestimation grows with increasing F and manifests itself apparently in an underestimation of the celerity in the diffusive wave approach. According to the numerical modelling results, the ratio of migration celerity of the diffusive wave model and the celerity of the full dynamic model changes from less than 1 to over 1 when the value of F increases. This change from underestimation of the celerity to overestimation of the celerity by the diffusive wave approach does not proceed from the spatial-mode analysis. However, the change in this range of F matches the range in which the spatial-mode analysis overestimates the migration celerity, in case of the full dynamic model. For F $>$ 0.3, the temporal-mode linear stability analysis predicts the bed wave celerity of the full dynamic model progressively better than the spatial-mode linear stability analysis . For these conditions, plausibly, the temporal-mode analysis also better predicts the celerity ratio of the simplified models.

For the quasi-steady model the results from both the spatial-mode analysis and the temporal-mode analysis are close to the numerical results. The errors in the spatial-mode analysis for the full dynamic model and the quasi-steady model for F $>$ 0.3 are apparently equally large.

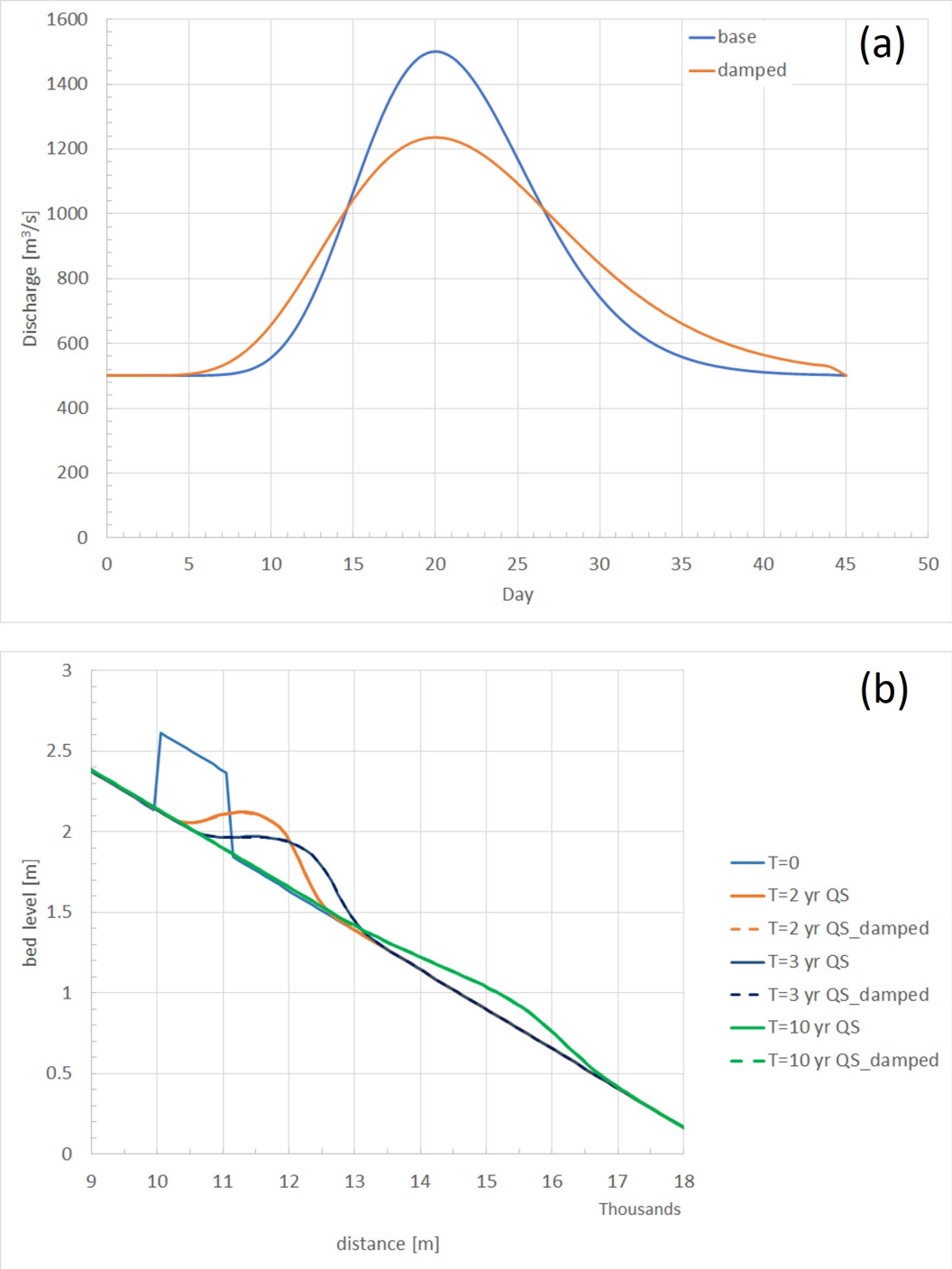

Figure 7. Simulations with the quasi-steady model for different flood waves as an upstream boundary condition. (a) original and attenuated flood wave with equal flood volume, (b) morphological response after 2, 3 and 10 years of simulation, with F=0.2 and $\Psi = 5.15 \cdot 10^{-5}$

.

Regarding the damping of bed perturbations the results of the temporal-mode analysis are in line with numerical modelling results (Figure 6). For the spatial-mode analysis this is also true for the quasi-steady approach. For the diffusive wave approach, the

underestimation of the damping is only partly captured by the spatial mode analysis for values of F larger than 0.4. Again, the deviation of the spatial-mode linear stability analysis estimates from numerical results for the full dynamic model in this range can explain this.

4.2 Quasi-Steady and Diffusive Wave Model

Overall, we conclude that the temporal-mode linear stability analysis results describe migration celerity and damping of bed waves in lowland rivers better than the spatial-mode equivalents. Based on this, a design graph can be constructed to assess the error of simplified models for various combinations of the parameters Froude number F, wave length L and transport parameter Ψ, as presented in Figure 8. Values of Ψ in a range from 0.005 to $5{\cdot}10^{-5}$ are adopted. In case of the Engelund-Hansen sediment transport predictor the range for the ratio s_o/q_o is then 0.001-$1{\cdot}10^{-5}$. The highest value could be considered a maximum. For the Yellow River the ratio is for example around 0.006. For lowland rivers such as the Meuse River, the Rhine River and the Po River the values of the ratio s_o/q_o are typically in the order of $1{\cdot}10^{-5}$.

Figure 8 shows that the quasi-steady model proves accurate for all combinations of these parameters. Only at the high values of Ψ a small deviation from 1 of the ratio for migration celerity and damping value can be observed. The diffusive wave model, which appears to be accurate for flood wave dynamics, deviates more than 5% from the full dynamic model for both migration and damping of bed waves when the Froude number is 0.2 or larger. The figure further shows that for this model (1) the results are insensitive to the magnitude of the sediment transport, (2) the wave length of the bed perturbation influences the ratio for the migration celerity, but not for the damping, and (3) the deviation from the full dynamic model increases with increasing Froude number.

4.3 Quasi-Steady Approach in Practise

Figure 7 shows that the impact of neglect of flood wave damping on morphological changes with the quasi-steady model may be small. This result is supported by simulations with a morphological model of the Meuse River, based on the numerical model SOBEK-RE. Sloff (2000) presented simulations for an extreme flood wave period with both the unsteady model and the quasi-steady model. Over 225 km of length the flood wave damping is moderate in the upstream 70 km long and relatively steep part of the river. In the transition area of around 20 km long, between steep and gentle longitudinal slope, large artificial lakes in the floodplains, created by sediment mining in the past, affect the shape of flood waves. Especially short spiky and average shaped flood waves are strongly dampened here. In Sloff (2000) the upstream model boundary was chosen just upstream of the transition area indicated above, so that the flood wave attenuation is included in the model. The unsteady model predicted bed level changes up to 1 m. The quasi-steady simulation for a 150 km long reach of the Meuse River could be performed using a 1 day time step instead of the 1/2 hour time step in the unsteady model. The run time of the quasi-steady model was consequently approximately 20 times shorter, but provided almost identical morphological effects in the main channel compared to the unsteady run (only few centimeters difference in some of the large peaks of morphological change). Apparently sediment transport gradients and morphological changes in the main channel at discharges exceeding bankfull conditions are hardly affected by the damping of flood waves. Due to the wide floodplains of the Meuse River and associated large conveyance capacity, the flow velocities in the main channel only increase to a limited extent above bankfull flow conditions. The sediment transport capacity in the main channel thus remains almost constant above bankfull flow and only the duration of exceedance of bankfull conditions is of importance. These results and the simulations described in Section 3.3 do not provide a generic indication of the applicability of quasi-steady models for long river reaches. For each application of a quasi-steady numerical model test

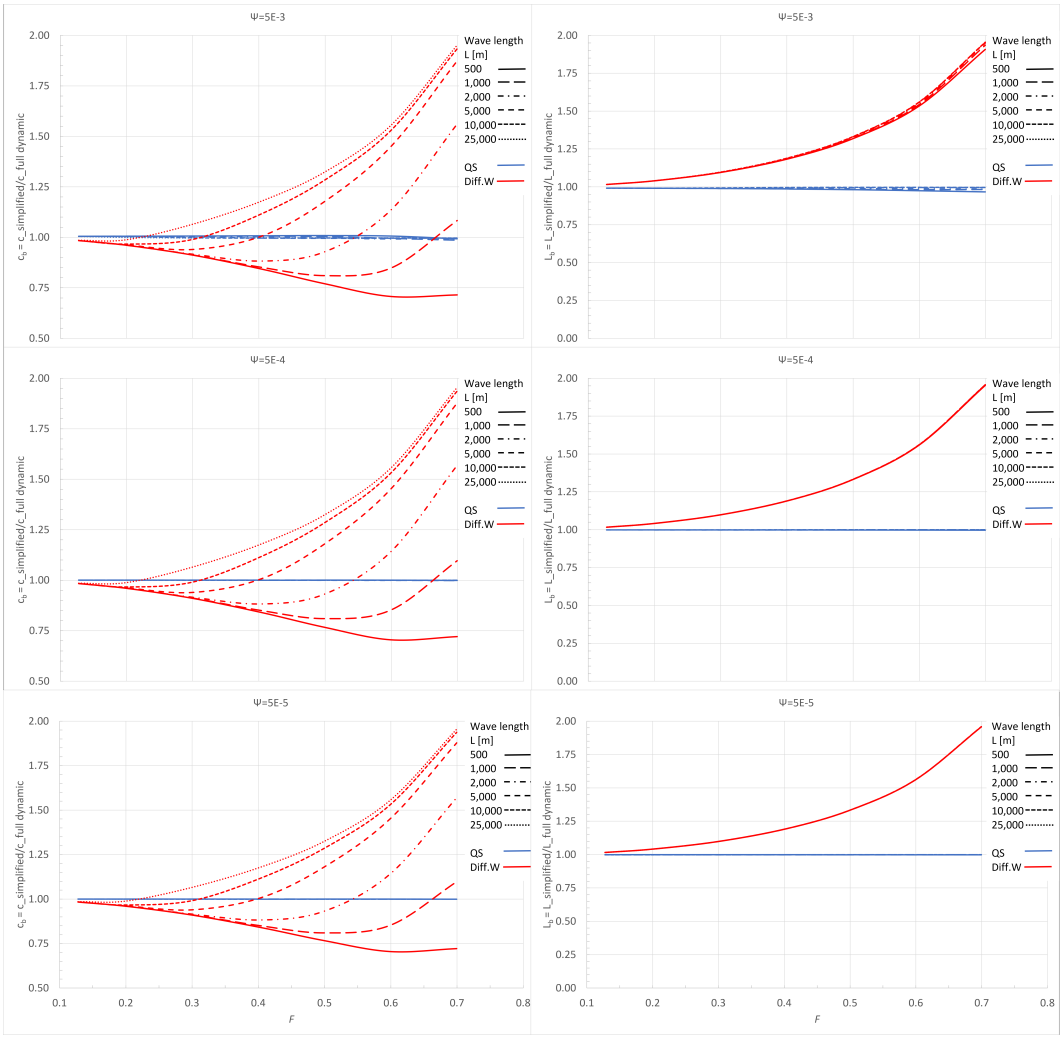

Figure 8. Ratio of migration celerities (left) and ratio damping length of simplified models to full dynamic model for different values of the sediment transport parameter Ψ: $5{\cdot}10^{-3}$ (top), $5{\cdot}10^{-4}$ (middle), $5{\cdot}10^{-5}$ (bottom).

simulations with both full dynamic model and quasi-steady model can help to decide whether the results with the simplified model are appropriate. If not, application of a quasi-steady model might still be feasible by simulating the flood wave attenuation with internal (boundary) conditions. An internal condition could take the form of lateral water inflow and extraction to represent the flood wave attenuation. Such an application of the quasi-steady model requires tailor-made assessment of the (internal) boundary conditions, especially when considering that the wave damping depends on the shape and peak value of each flood wave. For this assessment, the dimensions of the characteristics of the floodplains are also of importance (see example above for the Meuse River). With the above consideration in mind, the design graph of Figure 8 can be used to assess what kind of simplified model is accurate enough to be applied in general for the river reach considered. In case of the quasi-steady model some test simulations should be performed to determine whether (internal) boundary conditions should be implemented, so as to simulate the hydrodynamics in the complete model in such a way that the bed level evolution is accurately reproduced.

4.4 Other applications

The approach as presented is focused on one-dimensional river models, but could be applied to two- or three-dimensional models as well. In addition, it could be applied to other situations in which simplified models are often used, such as landscape evolution models. Tucker and Hancock (2010), Temme et al. (2013) and Nones (2020) for example describe that also for landscape evolution quasi-steady and diffusive wave models are often applied. The approach presented here with linear stability analyses and numerical modelling could indicate the applicability range of the simplified landscape evolution models as well.

5 Conclusions

The results of linear stability analyses and numerical simulations with ELV are compared to assess which type of linear stability analysis (temporal mode or spatial mode) best describes the impact of reducing the Saint Venant equations in morphodynamic simulations. The temporal-mode linear stability analysis outperforms the spatial-mode linear stability analysis in terms of predicting the the migration celerity of river bed waves. The same can be concluded for the damping length. The linear stability analysis results and the numerical simulations show that the quasi-steady model provides riverbed evolution results deviating less than 1% from the results with the full dynamic model for Froude numbers between 0.1 to 0.7, wave lengths of the bed waves up to 25,000 m and the non-dimensional sediment transport parameter Ψ from 0.005 to $5{\cdot}10^{-5}$. Previous calculations with high-complexity numerical models for long river sections indicate that, despite the neglect of attenuation of flood waves in quasi-steady models, morphological effects are well-predicted.

Although diffusive wave models are well-capable of simulating migration and damping of flood waves in lowland rivers, they underestimate or overestimate the migration celerity of bed waves. Especially the neglect of the convective acceleration term in this model causes this error. The degree of deviation is controlled by the Froude number F and the wave length of the bed perturbation L. Especially when F increases, diffusive wave models underestimate the damping of bed waves. Generally speaking, the migration celerity and damping of bed perturbations from the diffusive wave model deviate less than 5% from the full dynamic model when Froude numbers are 0.2 or less. To achieve at least 10% accuracy, the Froude number should not exceed 0.3.

Acknowledgments

This work is a part of the research program Rivers2Morrow (2018-2023), which focuses on long-term development of the Dutch rivers. Rivers2Morrow is financed by the Directorate-General for Water and Soil and Directorate-General Rijkswaterstaat, both being a part of the Dutch Ministry of Infrastructure and Water Management. HKV and Deltares provide additional support. We thank Dr. M. Borsboom and Dr. C. Sloff (both Deltares) for the valuable discussions on numerical aspects and the the merits of quasi-steady one-dimensional morphological models.

Data availability statement: Numerical simulations have been carried out with the numerical modelling package ELV. ELV is available in the open access repository of the Open Earth Tools managed by Deltares: https://svn.oss.deltares.nl/repos/openearthtools/trunk/matlab/applications/ELV. For the simulations we used the version at Revision 16973 from Thursday 17 December, 2020 11:20:54. The input and (reworked) output of the simulations with ELV, presented in the Figures 1 - 7, are available through Barneveld (2023).

References

Abril, J., Altinakar, M., & Wu, W. (2012). One-dimensional numerical modelling of river morphology processes with non-uniform sediment. In *River flow* (pp. 529–535).

Arkesteijn, L., Blom, A., Czapiga, M. J., Chavarrías, V., & Labeur, R. J. (2019). The quasi-equilibrium longitudinal profile in backwater reaches of the engineered alluvial river: A space-marching method. *Journal of Geophysical Research: Earth Surface*, *124*(11), 2542–2560.

Arkesteijn, L., Blom, A., & Labeur, R. J. (2021). A rapid method for modelling transient river response under stochastic controls with applications to sea level rise and sediment nourishment. *Journal of Geophysical Research: Earth Surface*, e2021JF006177.

Barneveld, H. (2023). Supplementary information for accuracy assessment of numerical morphological models based on reduced saint-venant equations, http://www.hydroshare.org/resource/a4f73ea96a574739b9b78f14f7a6c843.

Barneveld, H., Mosselman, E., Chavarrías, V., & Hoitink, A. (2023). Can linear stability analyses predict the development of riverbed waves with lengths much larger than the water depth? *Water Resources Research*, *59*(3).

Beg, M. N. A., Meselhe, E. A., Kim, D. H., Halgren, J., Wlostowski, A., Ogden, F. L., & Flowers, T. (2022). Diffusive wave models for operational forecasting of channel routing at continental scale. *JAWRA Journal of the American Water Resources Association*.

Blom, A., Arkesteijn, L., Chavarrías, V., & Viparelli, E. (2017). The equilibrium alluvial river under variable flow and its channel-forming discharge. *Journal of Geophysical Research: Earth Surface*, *122*(10), 1924–1948.

Cao, Z., Day, R., & Egashira, S. (2002). Coupled and decoupled numerical modeling of flow and morphological evolution in alluvial rivers. *Journal of Hydraulic Engineering*, *128*(3), 306–321.

Cao, Z., Xia, C., Pender, G., & Liu, Q. (2017). Shallow water hydro-sediment-morphodynamic equations for fluvial processes. *Journal of Hydraulic Engineering*, *143*(5), 02517001.

Cappelaere, B. (1997). Accurate diffusive wave routing. *Journal of Hydraulic Engineering*, *123*(3), 174–181.

Carraro, F., Vanzo, D., Caleffi, V., Valiani, A., & Siviglia, A. (2018). Mathematical study of linear morphodynamic acceleration and derivation of the MASSPEED approach. *Advances in Water Resources*, *117*, 40–52.

Charlier, J.-B., Moussa, R., David, P.-Y., & Desprats, J.-F. (2019). Quantifying peakflow attenuation/amplification in a karst river using the diffusive wave model with lateral flow. *Hydrological Processes*, *33*(17), 2337–2354.

Chavarrías, V., Arkesteijn, L., & Blom, A. (2019). A well-posed alternative to the Hirano active layer model for rivers with mixed-size sediment. *Journal of Geophysical Research: Earth Surface*, *124*(11), 2491–2520.

Chavarrías, V., Stecca, G., Siviglia, A., & Blom, A. (2019). A regularization strategy for modeling mixed-sediment river morphodynamics. *Advances in Water Resources*, *127*, 291–309.

Chen, T.-Y. K., & Capart, H. (2020). Kinematic wave solutions for dam-break floods in non-uniform valleys. *Journal of Hydrology*, *582*, 124381.

Church, M., & Ferguson, R. (2015). Morphodynamics: Rivers beyond steady state. *Water Resources Research*, *51*(4), 1883–1897.

Cimorelli, L., Cozzolino, L., D'Aniello, A., & Pianese, D. (2018). Exact solution of the linear parabolic approximation for flow-depth based diffusive flow routing. *Journal of Hydrology*, *563*, 620–632.

Dade, W. B., & Friend, P. F. (1998). Grain-size, sediment-transport regime, and channel slope in alluvial rivers. *The Journal of Geology*, *106*(6), 661–676.

De Vries, M. (1965). Considerations about non-steady bedload transport in open channels. In (p. 3-8).

De Vries, M. (1973). River bed variations-aggradation and degradation. In *Proc. int. seminars on hydr. of alluvial streams, iahr, delft, the netherlands* (pp. 1–10).

De Vries, M. (1975). A morphological time-scale for rivers. In *Deltares publication nr. 147, paper presented at the XVIth IAHR congress, São Paulo.*

DHI. (2017). *MIKE 11 - a modelling system for rivers and channels, reference manual.*

Drazin, P. G., & Reid, W. H. (2004). *Hydrodynamic stability.* Cambridge University Press.

Edmonds, D. (2012). Stability of backwater-influenced river bifurcations: A study of the Mississippi-Atchafalaya system. *Geophysical Research Letters*, *39*(8).

Engelund, F., & Hansen, E. (1967). A monograph on sediment transport in alluvial streams. *Teknisk Forlag, Kopenhagen.*.

Fan, P., & Li, J. (2006). Diffusive wave solutions for open channel flows with uniform and concentrated lateral inflow. *Advances in water resources*, *29*(7), 1000–1019.

Fasolato, G., Ronco, P., Langendoen, E., & Di Silvio, G. (2011). Validity of uniform flow hypothesis in one-dimensional morphodynamic models. *Journal of Hydraulic Engineering*, *137*(2), 183–195.

Fenton, J. D. (2019). Flood routing methods. *Journal of Hydrology*, *570*, 251–264.

Grijsen, J., & Vreugdenhil, G. (1976). Numerical representation of flood waves in rivers. *Proc. Int. Symp. Unsteady flow in open channels, Newcastle-upon-Tyne, BHRA Fluid Eng., Cranfield,.*

Guerrero, M., Latosinski, F., Nones, M., Szupiany, R. N., Re, M., & Gaeta, M. G. (2015). A sediment fluxes investigation for the 2-d modelling of large river morphodynamics. *Advances in Water Resources*, *81*, 186–198.

Haasnoot, M., Kwakkel, J. H., Walker, W. E., & Ter Maat, J. (2013). Dynamic adaptive policy pathways: A method for crafting robust decisions for a deeply uncertain world. *Global environmental change*, *23*(2), 485–498.

Habersack, H., Hein, T., Stanica, A., Liska, I., Mair, R., Jäger, E., ... Bradley, C. (2016). Challenges of river basin management: Current status of, and prospects for, the River Danube from a river engineering perspective. *Science of the Total Environment*, *543*, 828–845.

Harmar, O. P., Clifford, N. J., Thorne, C. R., & Biedenharn, D. S. (2005). Morphological changes of the Lower Mississippi River: geomorphological response to engineering intervention. *River Research and Applications*, *21*(10), 1107–1131.

Havinga, H. (2020). Towards sustainable river management of the Dutch Rhine River. *Water*, *12*(6), 1827.

Hummel, R., Duan, J. G., & Zhang, S. (2012). Comparison of unsteady and quasi-unsteady flow models in simulating sediment transport in an ephemeral arizona stream 1. *JAWRA Journal of the American Water Resources Association*, *48*(5), 987–998.

Lee, K. T., & Huang, P.-C. (2012). Evaluating the adequateness of kinematic-wave routing for flood forecasting in midstream channel reaches of Taiwan. *Journal of Hydroinformatics*, *14*(4), 1075–1088.

Lesser, G. R., Roelvink, J. v., Van Kester, J., & Stelling, G. (2004). Development and validation of a three-dimensional morphological model. *Coastal Engineering*, *51*(8-9), 883–915.

Lyn, D. A. (1987). Unsteady sediment-transport modeling. *Journal of Hydraulic Engineering*, *113*(1), 1–15.

Lyn, D. A., & Altinakar, M. (2002). St. Venant–Exner equations for near-critical and transcritical flows. *Journal of Hydraulic Engineering*, *128*(6), 579–587.

Meyer-Peter, E., & Müller, R. (1948). Formulas for bed-load transport. In *IAHSR 2nd meeting, Stockholm, Appendix 2.*

Mitsopoulos, G., Panagiotatou, E., Sant, V., Baltas, E., Diakakis, M., Lekkas, E., & Stamou, A. (2022). Optimizing the performance of coupled 1d/2d hydrodynamic models for early warning of flash floods. *Water*, *14*(15), 2356.

Morris, P. H., & Williams, D. J. (1996). Relative celerities of mobile bed flows with finite solids concentrations. *Journal of Hydraulic Engineering*, *122*(6), 311–315.

Moussa, R., & Bocquillon, C. (2009). On the use of the diffusive wave for modelling extreme flood events with overbank flow in the floodplain. *Journal of hydrology*, *374*(1-2), 116–135.

Nones, M. (2020). On the main components of landscape evolution modelling of river systems. *Acta Geophysica*, *68*(2), 459–475.

Olesen, K. (1981). *A numerical model for morphological computations in rivers with non-uniform sediment.* (Unpublished doctoral dissertation). Delft University of Technology, Faculty of Civil Engineering, Department of Hydraulic Engineering.

Paarlberg, A. J., Guerrero, M., Huthoff, F., & Re, M. (2015). Optimizing dredge-and-dump activities for river navigability using a hydro-morphodynamic model. *Water*, *7*(7), 3943–3962.

Ponce, V., & Simons, D. (1977). Shallow wave propagation in open channel flow. *Journal of the Hydraulics Division ASCE, Vol 103, HY12, Proc. Paper 13392, pp1461-1476*.

Ponce, V., & Simons, D. (1978). Shallow wave propagation in open channel flow. *Journal of the hydraulics Division ASCE, Vol 104, HY3, Proc. Paper 13635, pp 353-360.*.

Roelvink, J. (2006). Coastal morphodynamic evolution techniques. *Coastal Engineering*, *53*(2-3), 277–287.

Schuurman, F., & Kleinhans, M. G. (2015). Bar dynamics and bifurcation evolution in a modelled braided sand-bed river. *Earth Surface Processes and Landforms*, *40*(10), 1318–1333.

Sieben, J. (1996). One-dimensional models for mountain-river morphology. *Communications on hydraulic and geotechnical engineering, No. 1996-02*.

Singh, V. (2001). Kinematic wave modelling in water resources: a historical perspective. *Hydrological processes*, *15*(4), 671–706.

Siviglia, A., & Crosato, A. (2016). Numerical modelling of river morphodynamics: Latest developments and remaining challenges. *Advances in Water Resources*, *93*(Part A), 1–3.

Sloff, C. (2000). Morphological simulations Sand Meuse - Scope 2000, in Dutch: Morfologische berekeningen Zandmaas – Scope 2000. *Report WL Delft Hydraulics, Q2772, November 2022*.

Temme, A. J., Schoorl, J. M., Claessens, L., & Veldkamp, A. (2013). Quantitative modeling of landscape evolution.

Teng, J., Jakeman, A. J., Vaze, J., Croke, B. F., Dutta, D., & Kim, S. (2017). Flood inundation modelling: A review of methods, recent advances and uncertainty analysis. *Environmental modelling & software*, *90*, 201–216.

Tucker, G. E., & Hancock, G. R. (2010). Modelling landscape evolution. *Earth Surface Processes and Landforms*, *35*(1), 28–50.

USACE. (2022). *HEC-RAS River Analysis System, version 6.0, Hydrologic Engineering Center, User Manual V6.3.*

Van Buuren, R., Kuerten, H., & Geurts, B. J. (2001). Implicit time accurate simulation of unsteady flow. *International Journal for Numerical Methods in Fluids*, *35*(6), 687–720.

Vreugdenhil, C. (1982). Numerical effects in models for river morphology. *Engineering applications of computational hydraulics: Hommage to A. Preismann Vol. II: Numerical Models in Environmental Fluid Mechanics, Editors M.B. Abbott and J.A. Cunge*, *1*, 91–110.

Vreugdenhil, C. (1994). *Numerical methods for shallow-water flow* (Vol. 13). Springer Science & Business Media.

Williams, R., Measures, R., Hicks, D., & Brasington, J. (2016). Assessment of a numerical model to reproduce event-scale erosion and deposition distributions in a braided river. *Water Resources Research*, *52*(8), 6621–6642.

Ylla Arbós, C., Blom, A., Viparelli, E., Reneerkens, M., Frings, R., & Schielen, R. (2021). River response to anthropogenic modification: Channel steepening and gravel front fading in an incising river. *Geophysical Research Letters*, *48*(4), e2020GL091338.

Yossef, M. F., Jagers, H., Van Vuren, S., & Sieben, J. (2008). Innovative techniques in modelling large-scale river morphology. In *River Flow 2008, Proc. of the Intern. Conf. on Fluvial Hydraulics, Çeşme, Izmir, Turkey* (pp. 1065–1074).

Figure 1.

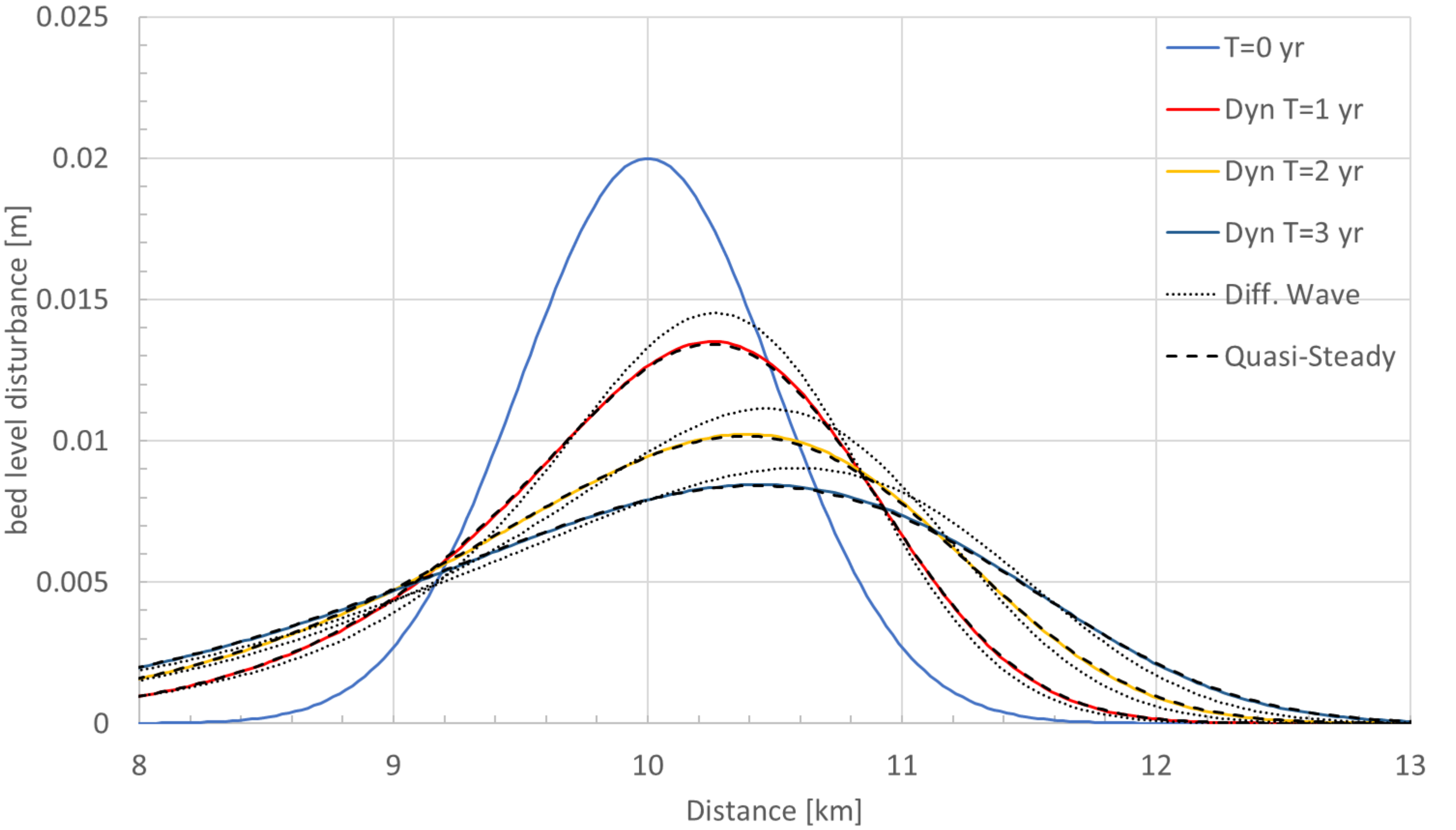
0.025
0.02
0.015
0.01
0.005
0
bed level disturbance [m]
8
9
10
11
12
13
Distance [km]
T=0 yr
Dyn T=1 yr
Dyn T=2 yr
Dyn T=3 yr
Diff. Wave
Quasi-Steady

Figure 2.

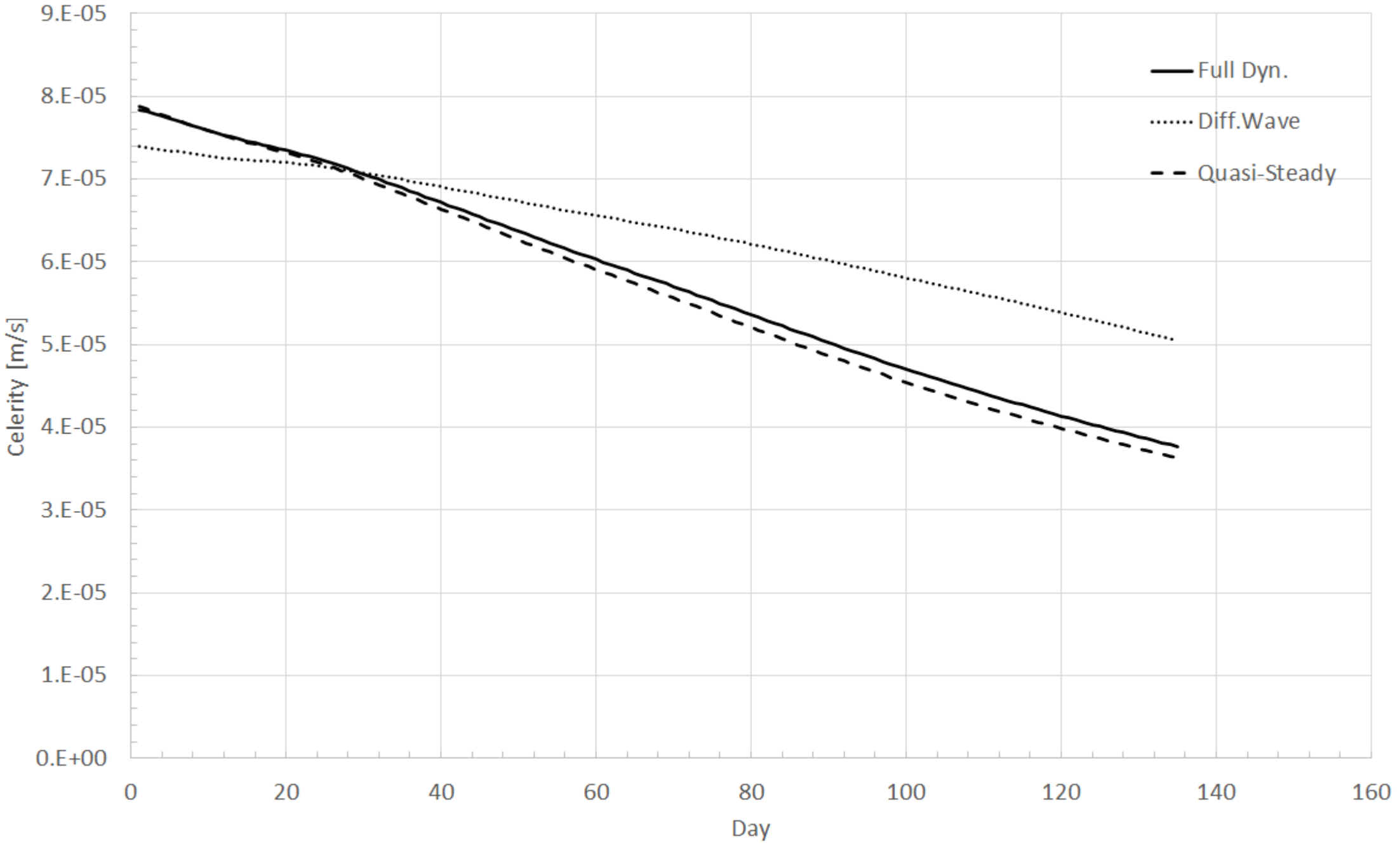
9.E-05
8.E-05
7.E-05
6.E-05
5.E-05
4.E-05
3.E-05
2.E-05
1.E-05
0.E+00
Celerity [m/s]
0
20
40
60
80
100
120
140
160
Day
Full Dyn.
Diff.Wave
Quasi-Steady

Figure 3.

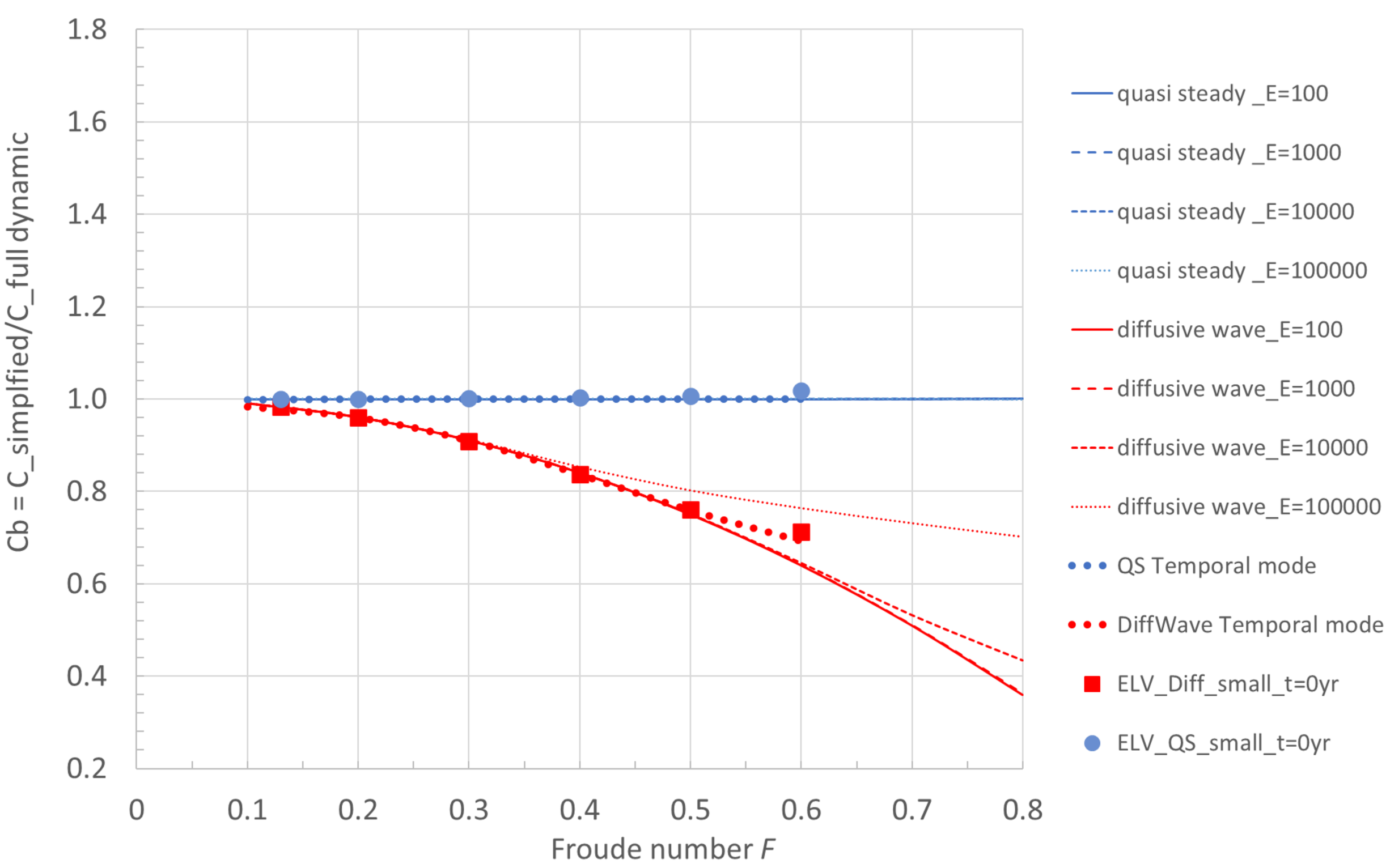
1.8
1.6
1.4
1.2
1.0
0.8
0.6
0.4
0.2
Cb = C_simplfied/C_full dynamic
0
0.1
0.2
0.3
0.4
0.5
0.6
0.7
0.8
Froude number F
quasi steady _E=100
quasi steady _E=1000
quasi steady _E=10000
quasi steady _E=100000
diffusive wave_E=100
diffusive wave_E=1000
diffusive wave_E=10000
diffusive wave_E=100000
QS Temporal mode
DiffWave Temporal mode
ELV_Diff_small_t=0yr
ELV_QS_small_t=0yr

Figure 4.

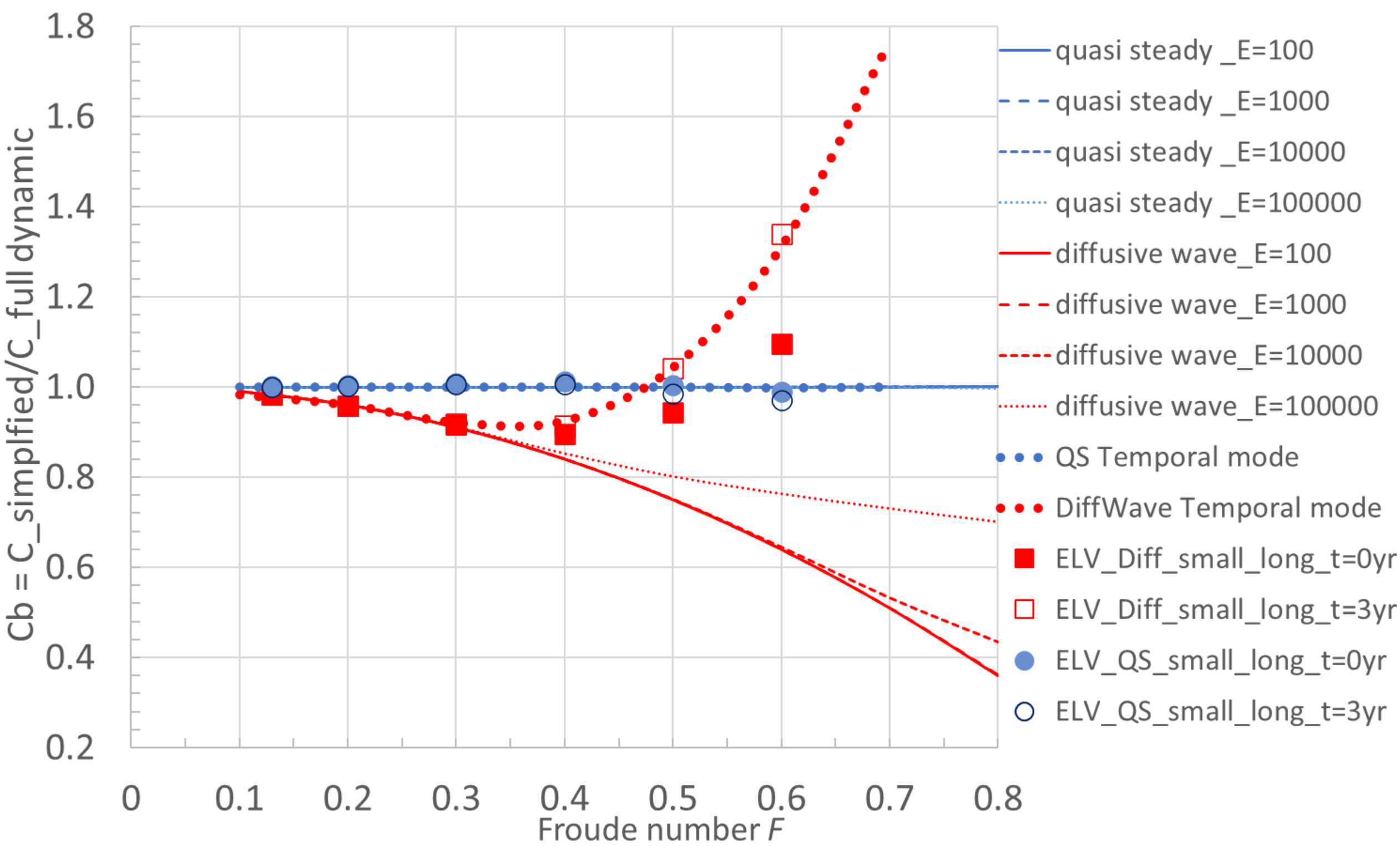
Cb = C_simplfied/C_full dynamic
1.8
1.6
1.4
1.2
1.0
0.8
0.6
0.4
0.2
0
0.1
0.2
0.3
0.4
0.5
0.6
0.7
0.8
Froude number F
quasi steady _E=100
quasi steady _E=1000
quasi steady _E=10000
quasi steady _E=100000
diffusive wave_E=100
diffusive wave_E=1000
diffusive wave_E=10000
diffusive wave_E=100000
QS Temporal mode
DiffWave Temporal mode
ELV_Diff_small_long_t=0yr
ELV_Diff_small_long_t=3yr
ELV_QS_small_long_t=0yr
ELV_QS_small_long_t=3yr

Figure 5.

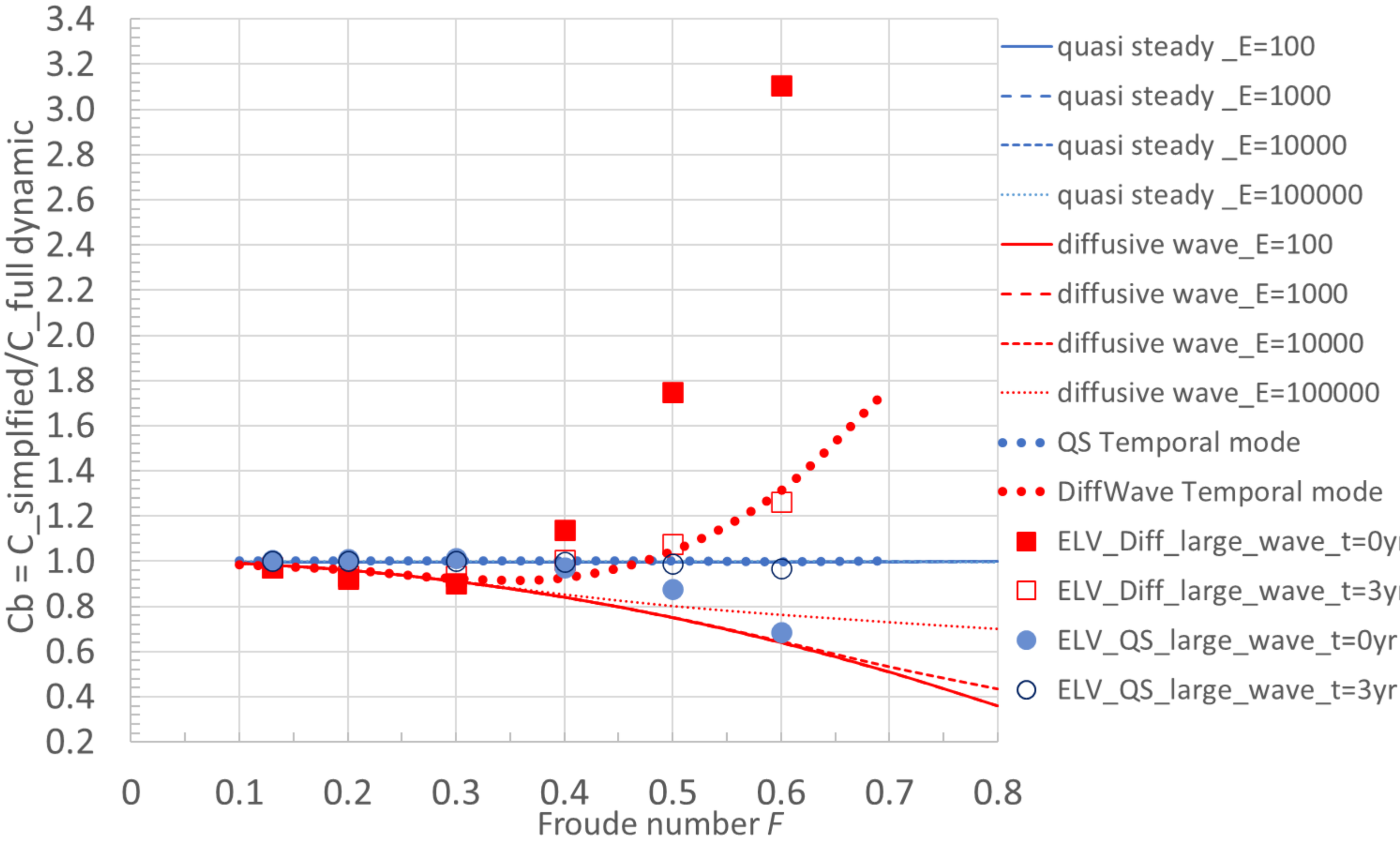
Cb = C_simplfied/C_full dynamic
3.4
3.2
3.0
2.8
2.6
2.4
2.2
2.0
1.8
1.6
1.4
1.2
1.0
0.8
0.6
0.4
0.2
0
0.1
0.2
0.3
0.4
0.5
0.6
0.7
0.8
Froude number F
quasi steady _E=100
quasi steady _E=1000
quasi steady _E=10000
quasi steady _E=100000
diffusive wave_E=100
diffusive wave_E=1000
diffusive wave_E=10000
diffusive wave_E=100000
QS Temporal mode
DiffWave Temporal mode
ELV_Diff_large_wave_t=0yr
ELV_Diff_large_wave_t=3yr
ELV_QS_large_wave_t=0yr
ELV_QS_large_wave_t=3yr

Figure 6.

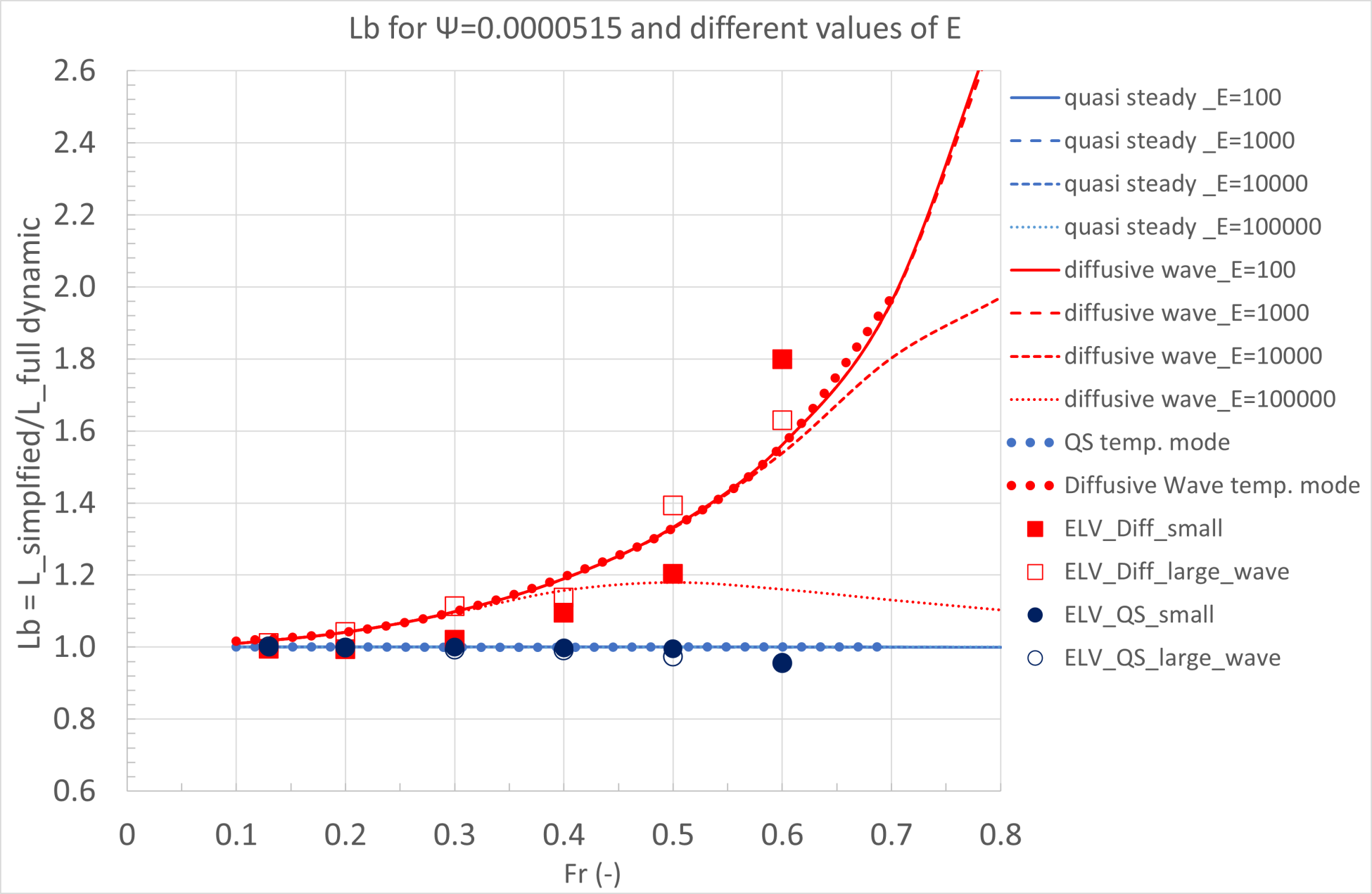
Lb for Ψ=0.0000515 and different values of E
Lb = L_simplfied/L_full dynamic
Fr (-)
2.6
2.4
2.2
2.0
1.8
1.6
1.4
1.2
1.0
0.8
0.6
0
0.1
0.2
0.3
0.4
0.5
0.6
0.7
0.8
quasi steady _E=100
quasi steady _E=1000
quasi steady _E=10000
quasi steady _E=100000
diffusive wave_E=100
diffusive wave_E=1000
diffusive wave_E=10000
diffusive wave_E=100000
QS temp. mode
Diffusive Wave temp. mode
ELV_Diff_small
ELV_Diff_large_wave
ELV_QS_small
ELV_QS_large_wave

Figure 7.

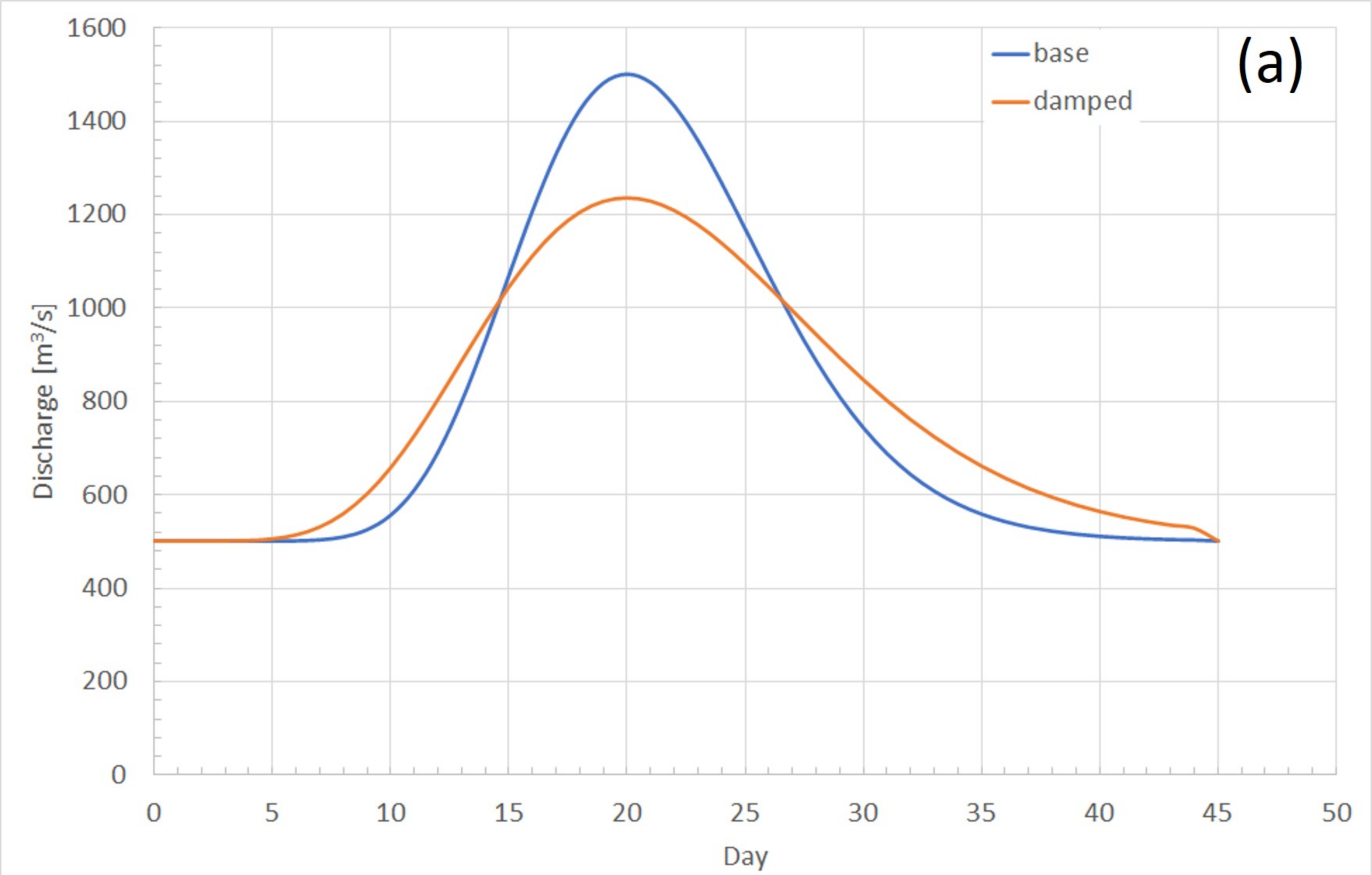
(a)
base
damped
Discharge [m³/s]
1600
1400
1200
1000
800
600
400
200
0
0
5
10
15
20
25
30
35
40
45
50
Day

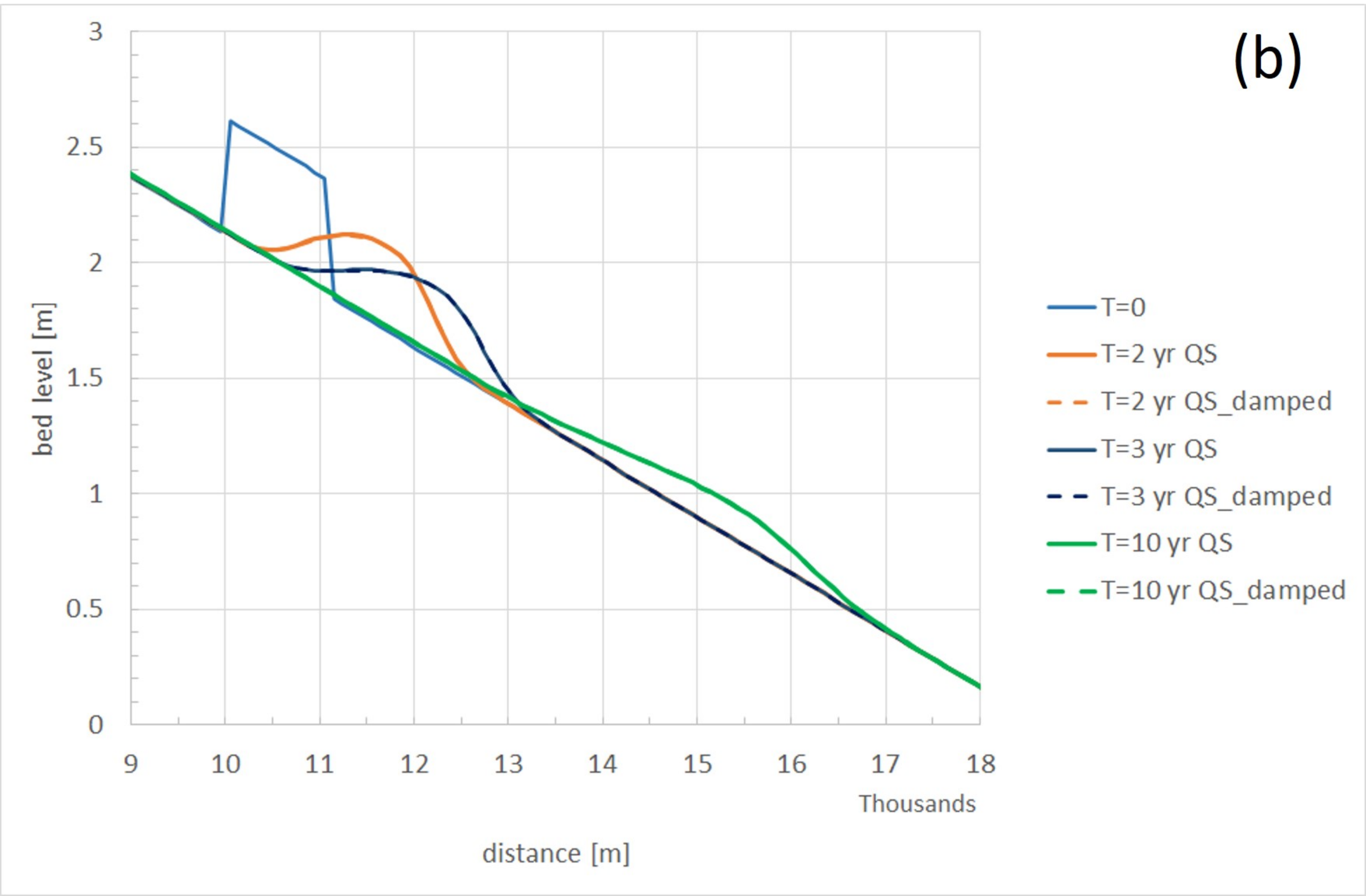
(b)
T=0
T=2 yr QS
T=2 yr QS_damped
T=3 yr QS
T=3 yr QS_damped
T=10 yr QS
T=10 yr QS_damped
bed level [m]
3
2.5
2
1.5
1
0.5
0
9
10
11
12
13
14
15
16
17
18
Thousands
distance [m]

Figure 8.

Ψ=5E-3

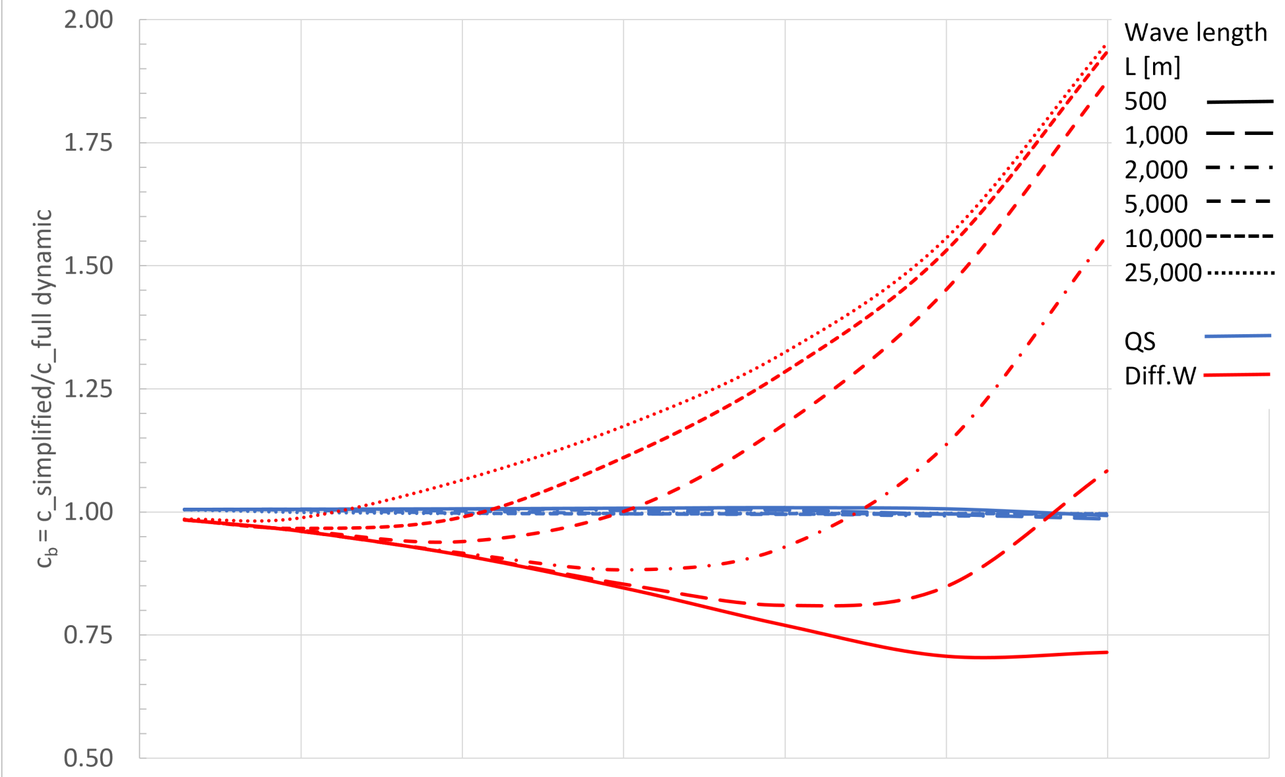

Ψ=5E-3

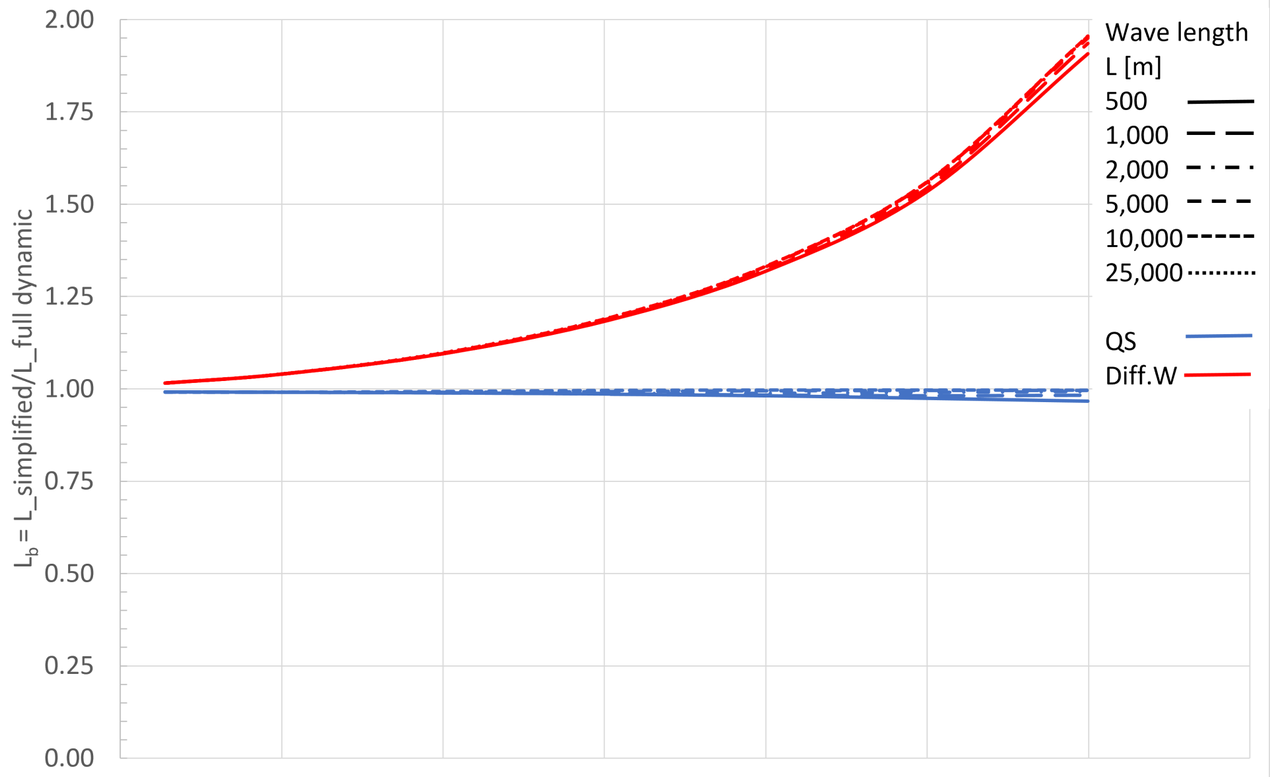

Ψ=5E-4

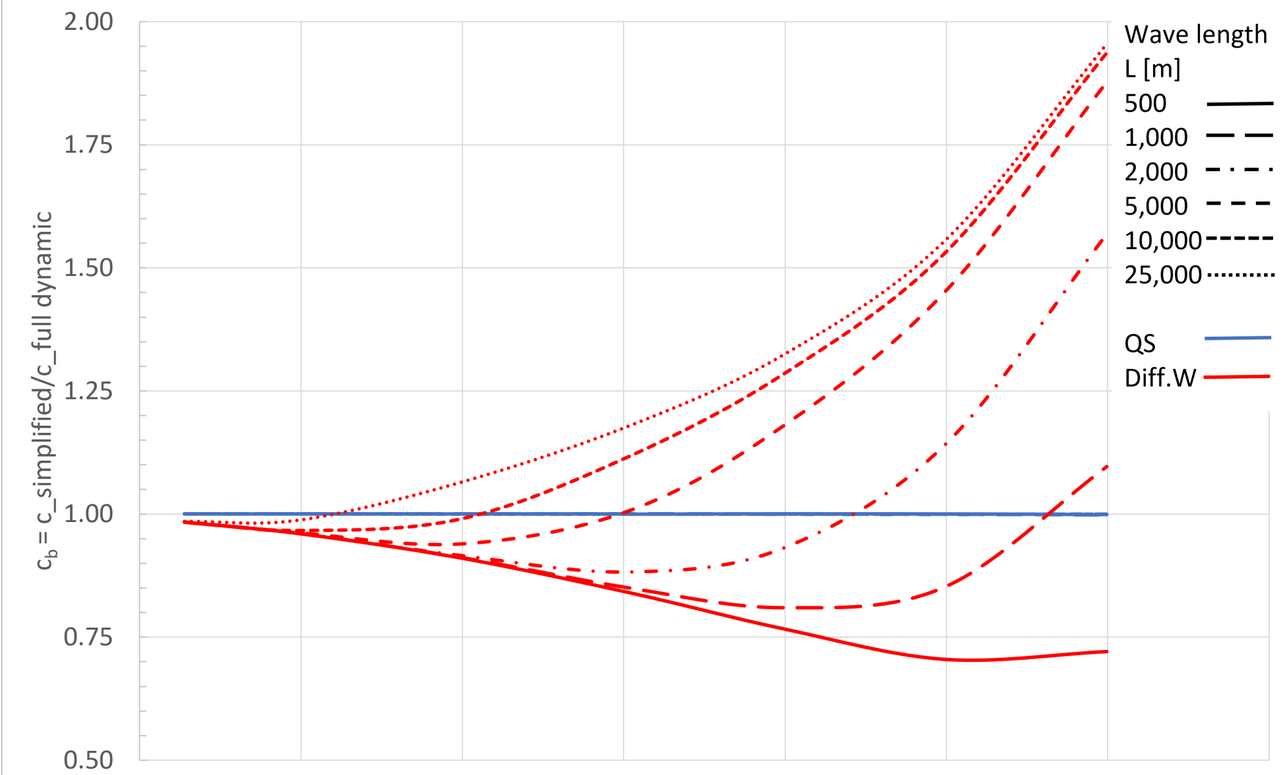

Ψ=5E-4

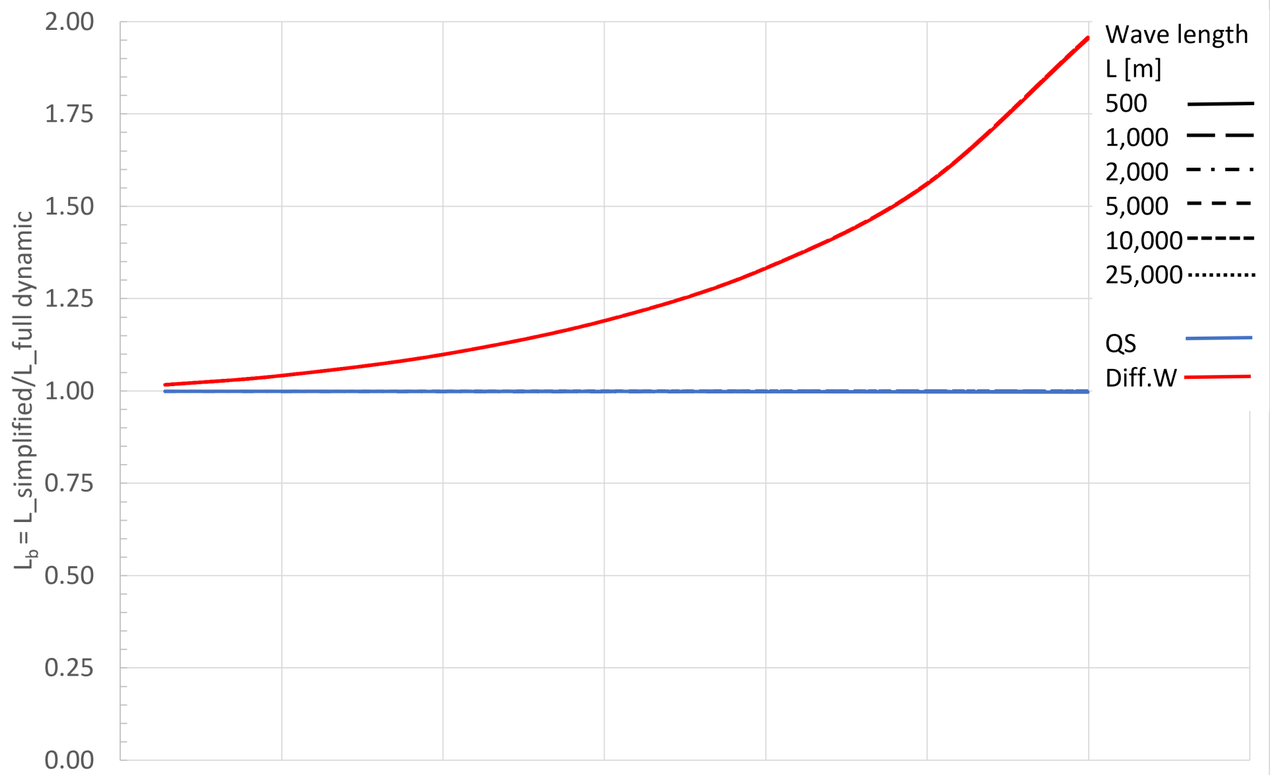

Ψ=5E-5

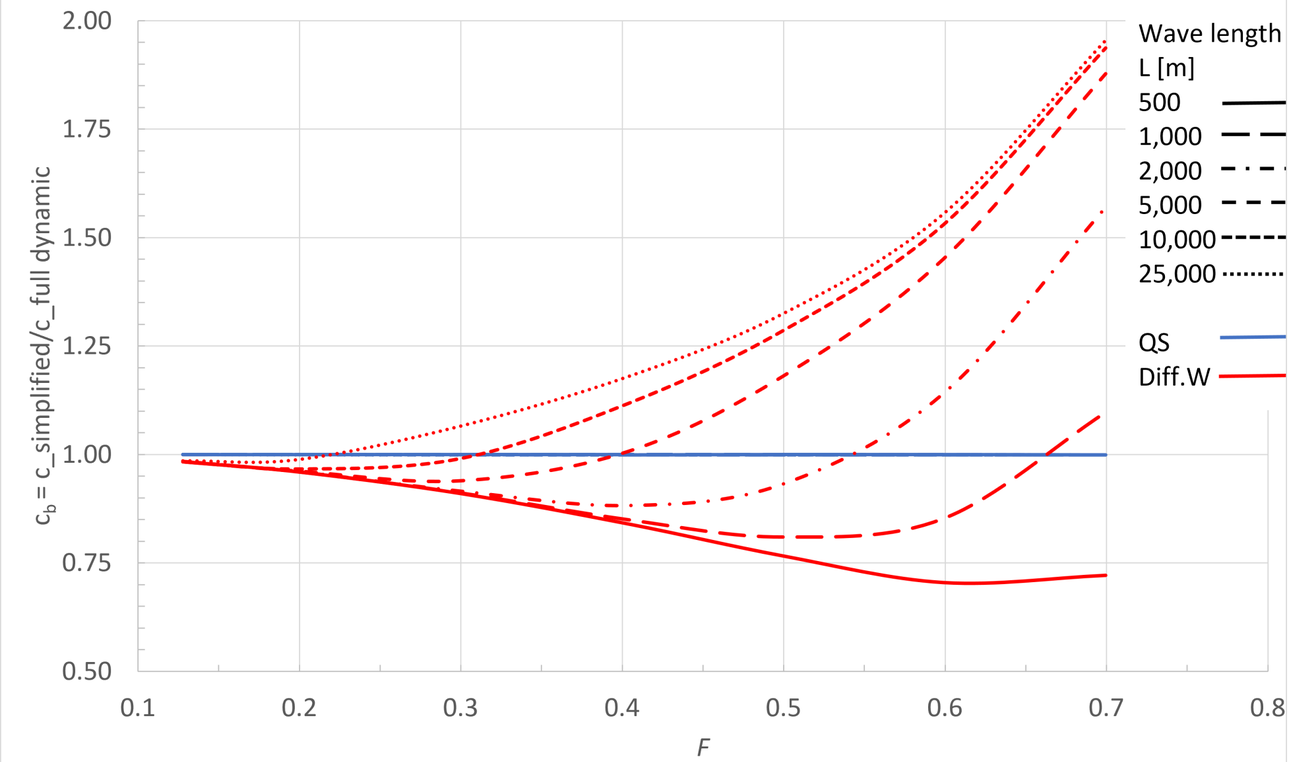

Ψ=5E-5